Chemical Geology 450 (2017) 59–80

Contents lists available at ScienceDirect

Chemical Geology

journal homepage: www.elsevier.com/locate/chemgeo

Was the Ediacaran Shuram Excursion a globally synchronized early diagenetic event? Insights from methane-derived authigenic carbonates in the uppermost Doushantuo Formation, South China

Huan Cui [a,b,*], Alan J. Kaufman [b], Shuhai Xiao [c], Chuanming Zhou [d], Xiao-Ming Liu [e]

[a] Department of Geoscience and NASA Astrobiology Institute, University of Wisconsin, Madison, WI 53706, USA
[b] Department of Geology and Earth System Science Interdisciplinary Center, University of Maryland, College Park, MD 20742, USA
[c] Department of Geosciences, Virginia Polytechnic Institute and State University, Blacksburg, VA 24061, USA
[d] Key Laboratory of Economic Stratigraphy and Palaeogeography, Nanjing Institute of Geology and Palaeontology, Chinese Academy of Sciences, Nanjing 210008, China
[e] Department of Geological Sciences, University of North Carolina, Chapel Hill, NC 27599, USA

ARTICLE INFO

Article history:
Received 6 July 2016
Received in revised form 4 December 2016
Accepted 5 December 2016
Available online 7 December 2016

Keywords:
Shuram Excursion
Authigenic carbonate
Early diagenesis
Ediacaran Period
Sulfate-Methane Transition Zone (SMTZ)
Anaerobic Oxidation of Methane (AOM)
Neoproterozoic Oxygenation Event (NOE)
$\delta^{13}C$ and $\delta^{18}O$ co-variation

ABSTRACT

The Ediacaran Period is characterized by the most profound negative carbon isotope ($\delta^{13}C$) excursion in Earth history, the Shuram Excursion. Various hypotheses – including the massive oxidation of dissolved organic carbon (DOC) in the oceans, the weathering of terrestrial organic carbon, or the release and oxidation of methane hydrates and/or expelled petroleum from the subsurface – have been proposed as sources of the ^{13}C-depleted carbon. More recently, it has been suggested that global-scale precipitation of early authigenic carbonates, driven by anaerobic microbial metabolism in unconsolidated sediments, may have caused the Shuram Excursion, but empirical evidence is lacking. Here we present a comprehensive analysis of a Shuram-associated interval from the uppermost Doushantuo Formation in South China. Our study reveals petrographic evidence of methane-derived authigenic calcite (formed as early diagenetic cements and nodules) that are remarkably depleted in ^{13}C – suggesting a buildup of alkalinity in pore fluids through the anaerobic oxidation of methane (AOM) – and systematically depleted in ^{18}O relative to co-occurring dolomite. Early authigenesis of these minerals is likely to be driven by increased microbial sulfate reduction, triggered by enhanced continental weathering in the context of a marked rise in atmospheric oxygen levels. In light of the finding of methane-derived authigenic carbonates at Zhongling, and based on our basin-scale stratigraphic correlation, we hypothesize that the marked ^{13}C and ^{18}O depletion (including their co-variation noted worldwide) in the Shuram Excursion may reflect an episode of authigenesis occurring within a sulfate–methane transition zone (SMTZ). If true, the Shuram Excursion was then a global biogeochemical response to enhanced seawater sulfate concentration in the Ediacaran ocean driven by the Neoproterozoic oxidation of surface environments. This paleo-oceanographic transition may have therefore paved the way for subsequent evolution and diversification of animals. Our study highlights the significance of an integrated approach that combines petrography, mineralogy, and texture-specific micro-drilling geochemistry in chemostratigraphic studies.

1. Introduction

On geological time scales, the global carbon cycle involves the exchange of carbon reservoirs between the atmosphere, the hydrosphere, and the deep mantle (Hayes and Waldbauer, 2006). The carbon flux derived from the mantle via volcanic outgassing is transferred to the rock record in the form of carbonates and organic carbon, which are subsequently subducted back into the deep Earth, thereby completing the long-term carbon cycle (Schidlowski, 1987; Hayes, 1994; Kump and Arthur, 1999).

Authigenic carbonates are not typically addressed in models of the global carbon cycle, although they could potentially be an important flux in carbonate burial and thus play an important role. Authigenesis (i.e., the process of authigenic mineralization) refers to any post-depositional processes, includes early diagenesis related to both seawater and meteoric alteration, or late diagenesis during deep burial. Authigenic carbonates formed during early diagenesis may be particularly important to the global carbon cycle insofar as they are normally formed under the influence of anaerobic microbial processes, including sulfate or iron reduction, which modify pore water chemistry and result in the dissolution, replacement, or cementation of pre-existing marine sediments (Berner, 1981; Kastner, 1999; Glenn et al., 2000; Lein, 2004; McMurtry, 2009). It has been suggested that modern authigenic carbonate accounts for at least 10% of global carbonate burial

* Corresponding author at: Department of Geoscience and NASA Astrobiology Institute, University of Wisconsin, Madison, WI 53706, USA.
E-mail address: Huan.Cui@wisc.edu (H. Cui).

http://dx.doi.org/10.1016/j.chemgeo.2016.12.010
0009-2541/

(Sun and Turchyn, 2014), and this proportion may have been significantly larger in Precambrian oceans (Schrag et al., 2013) given that these were incompletely oxygenated (Kah et al., 2004; Canfield et al., 2008; Lyons et al., 2014; Planavsky et al., 2014; Sperling et al., 2015; Liu et al., 2016).

Largely based on numerical modeling (Higgins et al., 2009), it was hypothesized that authigenic carbonates may have played a critical role in the Precambrian carbon cycle (Schrag et al., 2013). The Shuram Excursion in the Ediacaran Period (ca. 635–541 Ma) (Grotzinger et al., 2011; Xiao et al., 2016) presents an ideal opportunity to test this hypothesis. The Shuram Excursion in Oman is characterized by carbonate $\delta^{13}C$ values that plunge to a nadir of ca. −12‰ over a short stratigraphic interval and then rise steadily over hundreds of meters before recovering to baseline values (Burns and Matter, 1993; Fike et al., 2006; Le Guerroué, 2006). This profound carbon cycle anomaly is further characterized by: (1) covariations of carbon and oxygen isotopes in carbonates (Derry, 2010a; Grotzinger et al., 2011), (2) decoupling between carbonate carbon and organic carbon isotope compositions (Fike et al., 2006; McFadden et al., 2008; Lee et al., 2013), (3) a strong negative $\delta^{34}S$ excursion recorded in both pyrite and carbonate-associated sulfate (CAS) (Fike et al., 2006; Kaufman et al., 2007; McFadden et al., 2008), and (4) a progressive increase in $^{87}Sr/^{86}Sr$ isotopes (Melezhik et al., 2009; Sawaki et al., 2010; Cui et al., 2015; Xiao et al., 2016). This negative $\delta^{13}C$ excursion may result from the influence of ^{13}C-depleted authigenic carbonates (Macdonald et al., 2013; Schrag et al., 2013; Cui et al., 2016c), but to evaluate this possibility requires new detailed petrographic and geochemical data.

A pronounced negative $\delta^{13}C$ excursion in the uppermost Doushantuo Formation in the Yangtze Gorges area of South China is widely regarded as an equivalent of the Shuram Excursion (Jiang et al., 2007; McFadden et al., 2008; Lu et al., 2013; Tahata et al., 2013; Zhu et al., 2013; Wang et al., 2016; Xiao et al., 2016). However in outer-shelf environment, this excursion is only expressed by a few negative $\delta^{13}C$ data points (Zhou and Xiao, 2007; Zhu et al., 2007; Li et al., 2010). It is the inconsistent chemostratigraphic expression of this excursion between intra-shelf and outer-shelf environments that drew our initial attention (Cui et al., 2015). In this study, we present a comprehensive sedimentological, petrographic, and geochemical analysis of carbonates in both depositional and authigenic phases preserved in the Doushantuo Formation at the outer-shelf Zhongling section, and explore the biogeochemical origin and potential causal link to the global Shuram Excursion.

2. Materials and methods

This study is focused on the Doushantuo Formation at two sections in South China including the intra-shelf Jiulongwan section at the Yangtze Gorges area and the outer-shelf Zhongling section in Hunan Province (Fig. 1). The detailed geology of these sections has been described in previous publications (see McFadden et al., 2008; Jiang et al., 2011; Cui et al., 2015; Cui et al., 2016c). The Jiulongwan section preserves a typical Shuram Excursion (i.e., the EN3 interval in McFadden et al., 2008), with carbonate $\delta^{13}C$ values consistently around −9‰ in the upper 50 m of the Doushantuo Formation. In contrast, the upper 50 m of the Doushantuo Formation at the Zhongling section is characterized by highly variable $\delta^{13}C$ values, with only a few data points reaching nadir values of ca. −5‰ (Zhu et al., 2007; Li et al., 2010; Cui et al., 2015). In the field, the upper 50 m of the Doushantuo Formation at Zhongling is mainly composed of intraclastic, oolitic, or fine-grained dolomitic facies associated with three discrete levels of phosphorite, suggesting deposition in an outer shelf carbonate shoal environment (Jiang et al., 2011; Cui et al., 2015) (Figs. 2, 3).

The entire Doushantuo Formation at Zhongling was systematically sampled at high stratigraphic resolution. Detailed sedimentological observations were made in the field. During sampling, we observed centimeter-scale, white-colored calcite nodules that are distributed along sedimentary bedding in dolostone or phosphorite facies, as well as distinct white-colored calcite cement among dolomitic or phosphatic intraclasts (Fig. 2G–J). Late stage calcite veins were also observed in the host carbonates, and they often cross-cut sedimentary bedding (Fig. 2G–H). To provide a texture-resolved chemostratigraphy, detailed petrographic observation (Figs. 3, 4) and geochemical analysis of micro-drilled powders (Figs. 5–7) were conducted. All isotope analyses were performed using routine methods (e.g., McFadden et al., 2008; Cui, 2015; Cui et al., 2015, 2016a, 2016b, 2016c), which are briefly outlined below.

Carbonate carbon ($\delta^{13}C_{carb}$) and oxygen ($\delta^{18}O_{carb}$) isotopes were measured by continuous-flow isotope ratio mass spectrometry in the Paleoclimate Laboratory at the University of Maryland (UMD). Samples loaded into 3.7 mL Labco Exetainer vials and sealed with Labco septa were flushed with 99.999% Helium and manually acidified at 60 °C. The CO_2 analyte gas was isolated via gas chromatography, and water was removed using a Nafion trap prior to admission into an Elementar Isoprime stable isotope mass spectrometer fitted with a continuous flow interface. Data were corrected via automated MATLAB scripting on the VPDB and LSVEC scale using periodic in-run measurement of international reference carbonate materials and in-house standard carbonates, from which empirical corrections for signal amplitude, sequential drift, and one or two-point mean corrections were applied (Evans et al., 2016). Both isotopes are reported relative to VPDB. Precision for both is routinely better than 0.1‰.

Strontium isotopes ($^{87}Sr/^{86}Sr$) were analyzed for selected limestone and calcite nodule samples at the UMD Thermal Ionization Mass Spectrometry (TIMS) Laboratory. Detailed method has been fully described in our previous publications (Cui et al., 2015, 2016a, 2016c). Final data have been corrected for instrumental fractionation using the standard value $^{86}Sr/^{88}Sr = 0.1194$. Repeated analysis of the NBS SRM987 standard yields an average value of $^{87}Sr/^{86}Sr = 0.710245 \pm 0.000011$ (2σ) during the analytical window.

Major and trace elemental abundances of micro-drilled carbonates in both depositional phases and authigenic phases were analyzed for a few representative samples in order to better evaluate the degree of diagenetic alteration. Aliquots of the micro-drilled carbonate powders were dissolved in 0.4 M HNO_3, centrifuged, and only analyzed for the solutions. Petrographic observations indicate that these powders were largely free of siliciclastics; any clays, if present, would not have been dissolved by the dilute acid. The resulting solutions were analyzed on a Thermo Scientific® iCAP-Q ICP-MS (Inductively Coupled Plasma – Mass Spectrometry) at the Carnegie Institution of Washington. Precision of these analyses as determined by repeated measurements of a house standard carbonate was <5% (2σ) for major elements with high concentrations and <10% (2σ) for the REEs.

In order to better evaluate the diagenetic effect and quantitatively constrain the mineralogical abundances, we also conducted detailed petrographic observation and mineralogical analysis of representative samples using backscattered electron (BSE) imaging, elemental mapping, quantitative X-ray powder diffraction (XRD), and cathodoluminescence (CL) imaging in the X-ray Crystallographic Center at UMD, the Geobiology Laboratory at Virginia Tech, and the CL Laboratory at the Smithsonian Institution.

3. Sedimentology, petrography, and paragenesis

Detailed petrographic observations (Figs. 3, 4) were conducted in order to reconstruct the paragenesis of multiple mineralogical phases in the Doushantuo Formation. In the samples studied here, the well-preserved dolostone or phosphorite includes intraclasts, peloids, and ooids (Fig. 3C–F), suggesting a shallow marine shelf depositional environment. Well-preserved sand-sized phosphatic ooids generally have homogeneous fine-grained phosphatic cores coated with multiple cortical layers of dolomicrite (Fig. 3E, F).

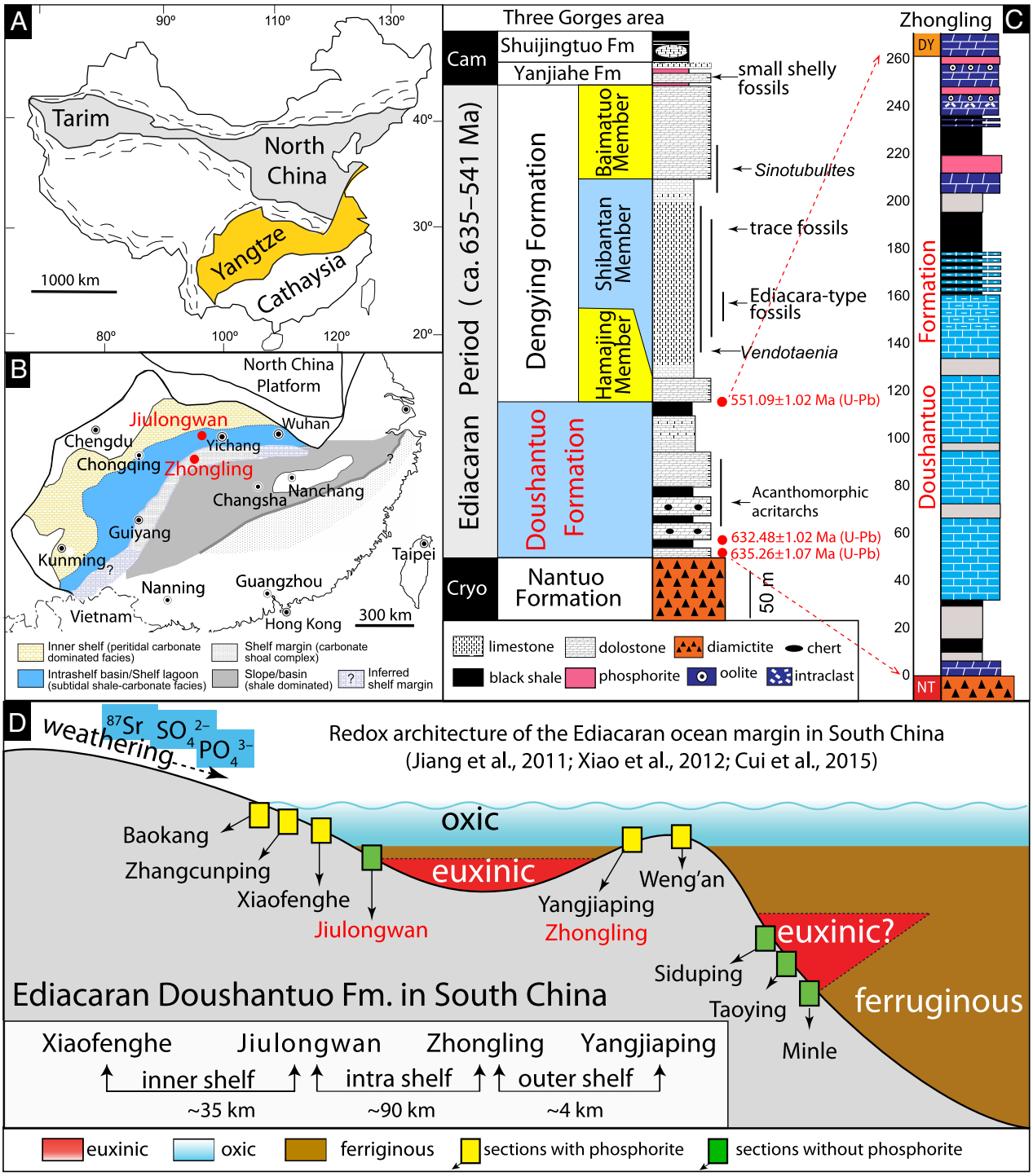

Fig. 1. (A) Geological map of China, with the Yangtze Craton in yellow. (B) Reconstructed Ediacaran depositional environments on the Yangtze Craton (Jiang et al., 2011). Red dots indicate the location of the Zhongling and Jiulongwan sections. (C) Simplified litho-, bio-, and chrono-stratigraphy of the Ediacaran Doushantuo and Dengying formations in South China. Modified from Chen et al. (2013) and Cui et al. (2016c). Radiometric ages from Condon et al. (2005) and Schmitz (2012). Thickness is not to scale. Cam = Cambrian; Cryo = Cryogenian. (D) Reconstructed redox architecture during the deposition of the upper Doushantuo Formation. Sedimentology (Jiang et al., 2011; Zhu et al., 2013) and chemostratigraphy (Cui et al., 2015; Wang et al., 2016) suggest that the Doushantuo Formation at Jiulongwan section was deposited in an intra-shelf environment, while the Zhongling section were deposited in an outer-shelf environment. The euxinic conditions on the platform were largely restricted in intra-shelf lagoonal settings (Cui et al., 2015), rather than an open shelf environment (Li et al., 2010). Sections with phosphorite deposits (e.g., inner shelf sections at Baokang, Zhangcunping, and Xiaofenghe; outer shelf sections at Zhongling, Yangjiaping and Weng'an) and without phosphorite deposits (e.g., intra-shelf section at Jiulongwan and slope section at Siduping, Taoying, and Minle) are marked in different symbols for reference. Modified from Cui et al. (2016c).

Based on the occurrence of phosphatic allochems and oolite, the bedded fine-grained dolostone and phosphorite were likely to have formed in well agitated seawater, and then dolomitized in the outer-shelf environment prior to lithification. Like most well-preserved Proterozoic dolostones, the Doushantuo dolostones are pervasively fine-grain sized, which are here interpreted to record either primary precipitation, or very early dolomitization in marine environments (Tucker, 1982, 1983; Tucker and Wright, 1990). No mineralogical evidence for the metamorphic growth of silicate mineral phases was observed in the thin sections.

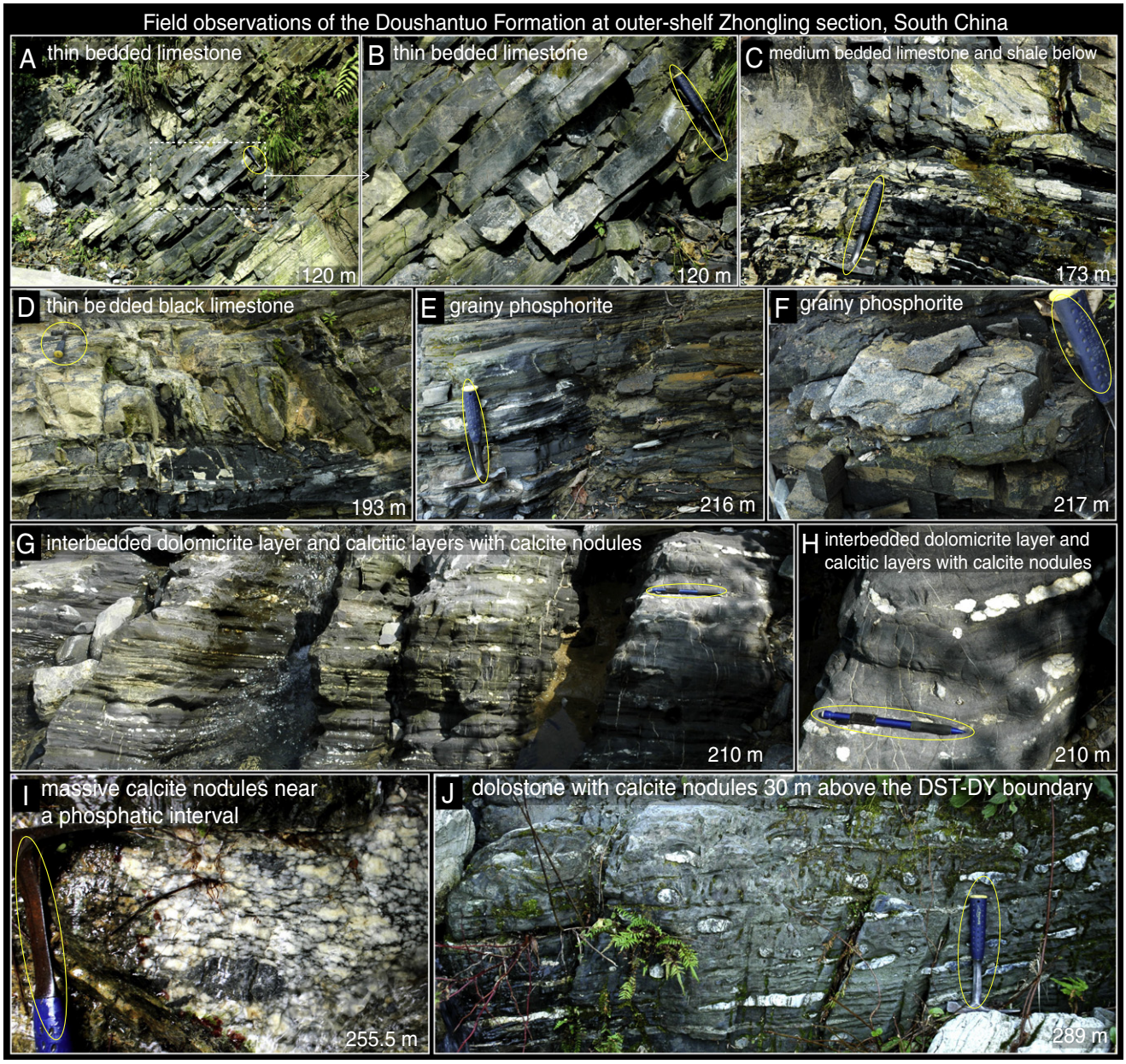

Fig. 2. Sedimentological observation of the Doushantuo Formation at the outer-shelf Zhongling section, South China. The numbers in the lower right represent stratigraphic heights in the Doushantuo Formation above the Marinoan (Nantuo) diamictite. Scales are circled in each view. (A) Bedded limestones of the middle Doushantuo Formation (rock hammer for scale). (B) A closer view of marked area in A. (C) Medium bedded limestone and overlying mudstone. (D) Thin bedded black limestone and overlying mudstone. (E, F) Grainy phosphorite interval. (G, H) Stream exposure reveals interbedded calcitic and dolomitic layers with abundant white calcite nodules along sedimentary bedding. Late-stage calcite veins are also visible in this view, but are mostly irregularly distributed and cross cut bedding planes (pencil for scale). (I) Massive white-colored calcite nodules surrounded by silica within a phosphorite horizon. (J) Lens-shaped authigenic calcite interbedded with the lower Dengying dolostone.

To various degrees, the phosphorite and dolostone were dissolved, replaced, and cemented by authigenic quartz and calcite (Fig. 4). The most distinct feature we observed in the field is the occurrence of white-colored calcite nodules aligned with sedimentary bedding in the uppermost Doushantuo and lower Dengying formations (Fig. 2G–J). These calcite nodules are primarily composed of coarse euhedral calcite crystals, which appear as coalesced patches under microscopic observation. Coarse calcite also fill remaining voids among intraclasts and ooids (Fig. 4). Most of the calcite nodules are lined with a silica rim. Quartz crystals in the rim grow centripetally inward towards the center of the nodule, suggesting that they formed prior to, or simultaneously with the calcite (e.g., Xiao et al., 2010; Cui et al., 2016c). Under CL microscopy, the calcite phase is dull and quartz is black (Fig. 4I). It is also notable that disseminated pyrite is widespread in the studied samples (Fig. 3H, I) (Cui et al., 2016c).

Based on the above petrographic observation, together with similar observation in the nearby Yangjiaping section ~4 km to the east (Cui et al., 2015, 2016c), we reconstruct the following paragenetic sequence. (1) Dissolved phosphate in the water column was transported to the marine sediments via the "Fe–P shuttle" (Shaffer, 1986; Glenn et al., 1994; Muscente et al., 2015; Cui et al., 2016c). The release of Fe-bound phosphorous in the iron reduction zone after deposition raised pore-water phosphate saturation levels, resulting in the precipitation of authigenic phosphate along with dolomite. (2) The presence of phosphatic intraclasts and oolitic dolostone suggests sedimentary reworking

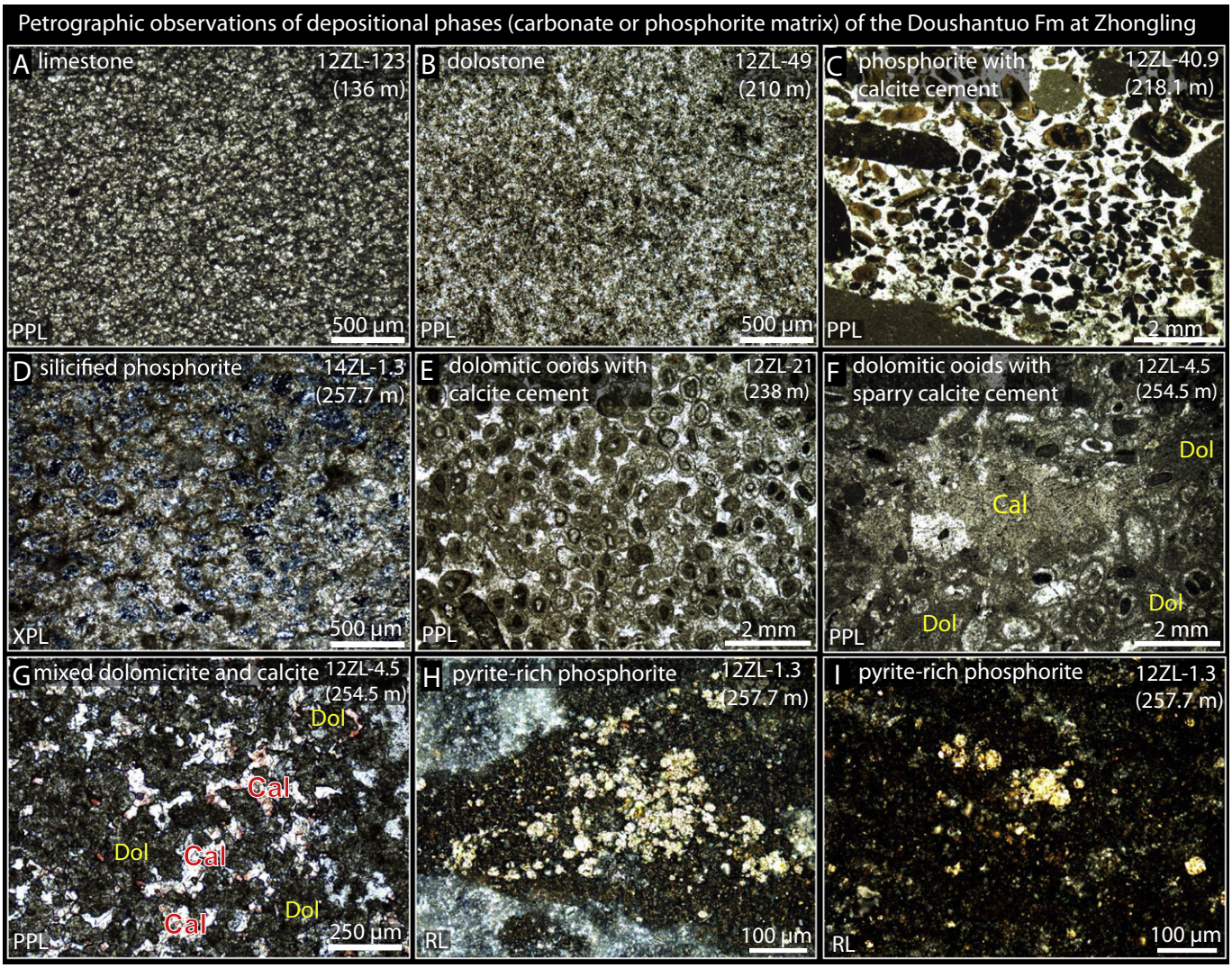

Fig. 3. Petrographic images of the Doushantuo Formation at the Zhongling section, showing the main features of carbonate matrix in the studied samples. Numbers (e.g., 136 m) below sample names in the upper right represent the stratigraphic height above the Marinoan (Nantuo) diamictite at the Zhongling section. PPL = plane polarized light; XPL = cross polarized light. (A, B) Homogenous micritic limestone and fine-grained dolostone, respectively. (C) Phosphorite intraclasts cemented by calcite. (D) Silicified phosphorite under XPL. Phosphorite grains are preferentially silicified. (E) Dolomitic ooids cemented by white calcite. (F) Sparry calcite cement in the dolomitic oolite. (G) Mixed dolomicrite (dark) and calcite (white or red, stained by Alizarin-red S) in a limestone layer of a dolostone sample. (H, I) Disseminated pyrite in phosphorite under reflective light (RL).

and local transportation in a high-energy shoal environment. (3) After final deposition, these allochems were cemented by authigenic calcite, or replaced by authigenic calcite and quartz as distinct nodules forming along bedding planes. (4) Late-stage calcite veins also occur in some intervals, which cross cut sedimentary bedding planes and must have formed after the sediments were lithified. In summary, the Doushantuo samples from the shallow outer-shelf region at Zhongling recorded primary depositional and authigenic events in the sedimentary environment.

4. Geochemical results

4.1. Geochemical analysis by micro-drilling

After petrographically characterizing the sedimentary textures and minerals, various carbonate fabrics were micro-drilled and analyzed for $\delta^{13}C$ and $\delta^{18}O$ compositions (Figs. 5–7, Tables S1–2) in order to construct chemostratigraphic profiles (Fig. 8). Within the scale of a single hand sample, we find marked heterogeneity in both $\delta^{13}C$ and $\delta^{18}O$ compositions. The $\delta^{13}C$ of authigenic calcite phases reveals extraordinarily negative values, ranging from ca. −5 to as low as −37‰, whereas the dolomitic or phosphatic matrices ranges from ca. −2 to +7‰. Similarly, authigenic calcite phases preserve more negative $\delta^{18}O$ values (ca. −9‰) compared with depositional phases (ca. −5‰). The lower 200 m of the Doushantuo Formation at the Zhongling section (Fig. 2A–D) have also been carefully investigated, but no distinct calcite nodules were found at lower levels (Fig. S1). Thus, the phase-correlated $\delta^{13}C_{carb}$ and $\delta^{18}O_{carb}$ heterogeneity is only restricted to the upper 60 m of the Zhongling section (Fig. 8J, K).

Elemental concentration and strontium isotope analyses were also conducted on representative samples in order to compare primary depositional and secondary authigenic phases and to evaluate the overall degree of diagenetic alteration. In this regard, both dolomite matrices and authigenic calcites were micro-drilled. In all the analyzed samples, authigenic calcites had significantly higher Sr concentration and much lower Fe, Mn, and Rb concentration when compared with the dolomite matrix (Table S3). In addition, $^{87}Sr/^{86}Sr$ compositions of the authigenic white calcite nodules and cements (ranging from 0.7080 to 0.7083 among all samples) are typically less radiogenic than the dark-colored dolomitic phase (range from 0.7080 to 0.7088 among all samples) in which they are hosted (Figs. 5A, 6A, B, 9A).

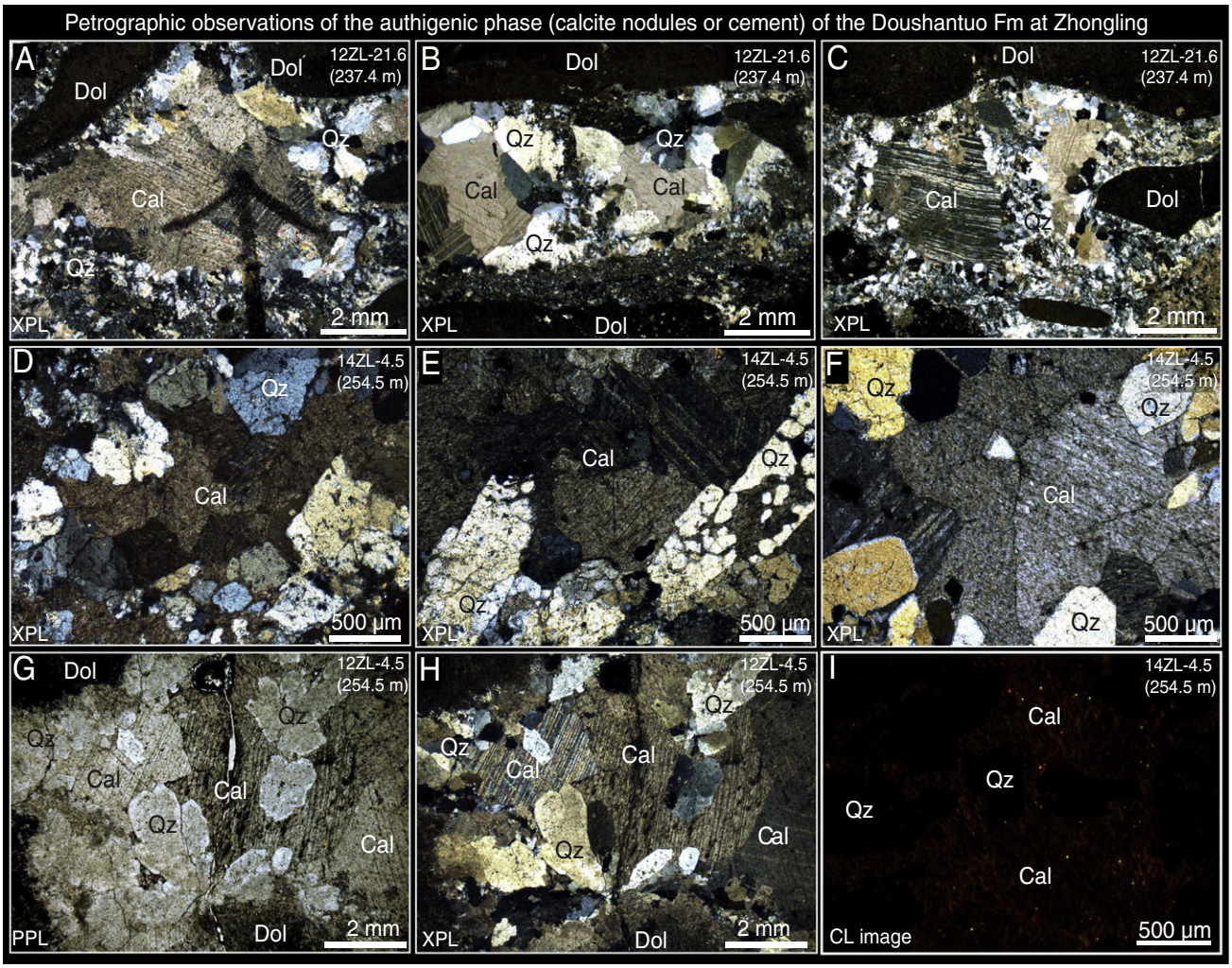

Fig. 4. Petrographic observation of samples from the Doushantuo Formation at the Zhongling section, showing the main features of authigenic calcite in the studied samples. Numbers below sample names in the upper right represent the stratigraphic height above the Marinoan (Nantuo) diamictite at the Zhongling section. PPL = plane polarized light; XPL = cross polarized light. (A–C) Petrographic images showing void-filling calcite cements surrounded by quartz in an intraclastic dolostone sample. Quartz crystals in the silica rim grow centripetally towards the calcite void-filling cements, suggesting that they formed before or simultaneously with the calcite. Calcite phase in this sample has $^{87}Sr/^{86}Sr$ value of 0.70811, whereas a dolomite intraclast in this sample has a slightly higher $^{87}Sr/^{86}Sr$ value of 0.70879. (D–H) Petrographic images showing void-filling calcite cements co-occurring with quartz in a dolomitic phosphorite sample. Some quartz crystals are replaced by calcite in later-stage diagenesis. Quartz crystals in the silica rim grow centripetally towards the calcite void-filling cements, suggesting that they formed before or simultaneously with the calcite. Calcite phase in this sample (14ZL–4.5) has $^{87}Sr/^{86}Sr$ value of 0.70827. Images G and H show the same view under PPL and XPL, respectively. (I) Cathodoluminescence (CL) image of calcite and quartz in a calcite nodule. Both show dim color under CL light. Cal = calcite; Dol = dolomite; Qz = quartz.

4.2. Compiled chemostratigraphic profiles

The chemostratigraphic data are plotted using different symbols in the illustrations so that different texture, mineralogy, and paragenetic stages can be better distinguished and evaluated during interpretation. Chemostratigraphic profiles of the Doushantuo Formation at the intra-shelf Jiulongwan section and outer-shelf Zhongling section reveal many similarities, but also some distinct variations. For example, the $\delta^{13}C_{carb}$ profile of the Doushantuo at Jiulongwan (Fig. 8A) shows three pulsed Ediacaran Negative (EN) excursions: EN1 in the basal cap carbonate, EN2 in the middle section, and EN3 at the top (McFadden et al., 2008). EN2 has been proposed to be correlated with the middle Ediacaran Gaskiers glaciation (Tahata et al., 2013), although this age assignment remains a matter of intense debate (Narbonne et al., 2012; Xiao et al., 2016). EN3 is widely regarded as an equivalent of the Shuram Excursion recognized worldwide (Jiang et al., 2007; McFadden et al., 2008; Grotzinger et al., 2011). However, the $\delta^{13}C_{carb}$ profile of typical marine carbonates at Zhongling reveals only a few scattered and moderately negative data points (Fig. 8J). Plotting our data from authigenic calcite phases, the integrated $\delta^{13}C_{carb}$ profile at Zhongling reveals three distinct intervals with extremely negative $\delta^{13}C_{carb}$ values (Fig. 8J). The $\delta^{18}O_{carb}$ profile of the EN3 interval at Jiulongwan show an overall negative excursion down to −10‰, which broadly co-varies with the $\delta^{13}C_{carb}$ profile (Fig. 8B). In contrast, the $\delta^{18}O_{carb}$ profile at Zhongling preserves three small and discrete negative excursions corresponding to the three negative $\delta^{13}C_{carb}$ spikes (Fig. 8K).

Compared to the record of carbonate carbon isotope variations, the $\delta^{13}C_{org}$ profile at Jiulongwan is generally invariant with ca. −30‰ values through most of the section, with the exception of an abrupt decrease down to almost −40‰ in the uppermost black shale interval (Fig. 8C) (McFadden et al., 2008). At Zhongling, the $\delta^{13}C_{org}$ profile in the lower 40 m shows an overall increase that parallels the corresponding $\delta^{13}C_{carb}$ profile, and then remains steady at ca. −25‰, with only a slight decrease towards the top of the section (Fig. 8L). It is notable that the $\delta^{13}C_{carb}$ and $\delta^{13}C_{org}$ profiles at the uppermost Doushantuo Formation are decoupled, which has similarly been observed in Shuram equivalent strata in Oman (Fike et al., 2006; Lee et al., 2013; Lee et al., 2015) and Australia (Calver, 2000).

Sulfur and strontium isotope profiles in the inner and outer shelf sections also reveal significant differences. The $\delta^{34}S$ profiles based on both

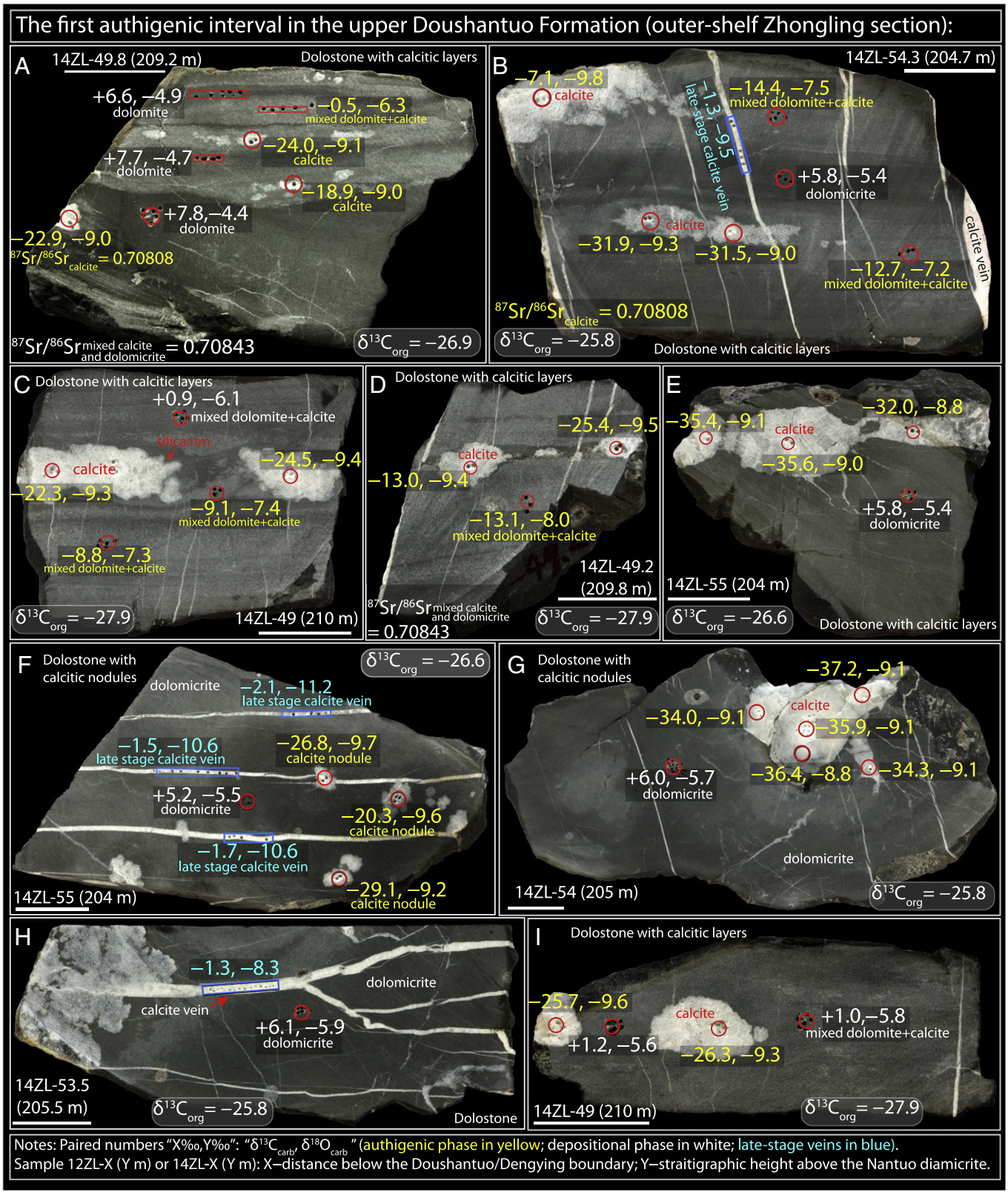

Fig. 5. Paired carbonate carbon and oxygen isotope data for micro-drilled spots in samples from the first stratigraphic interval of authigenic calcite in the Doushantuo Formation at the Zhongling section. See Fig. 8J for the stratigraphic position of the three intervals of authigenic calcite. Each pair of data shows $\delta^{13}C_{carb}$ (‰, VPDB) and $\delta^{18}O_{carb}$ (‰, VPDB), respectively. Organic carbon isotope ($\delta^{13}C_{org}$, VPDB) data of bulk acidified residues are also given for each sample. All scale bars are 2 cm long. Sample names were provided together with the scale bars. Stratigraphic height above the Marinoan (Nantuo) diamictite for each sample is provided in parentheses after each sample name. Yellow, white, and blue labels represent authigenic calcite phases, depositional phases, and late-stage veins, respectively. $^{87}Sr/^{86}Sr$ values are also shown for selected spots and samples when available.

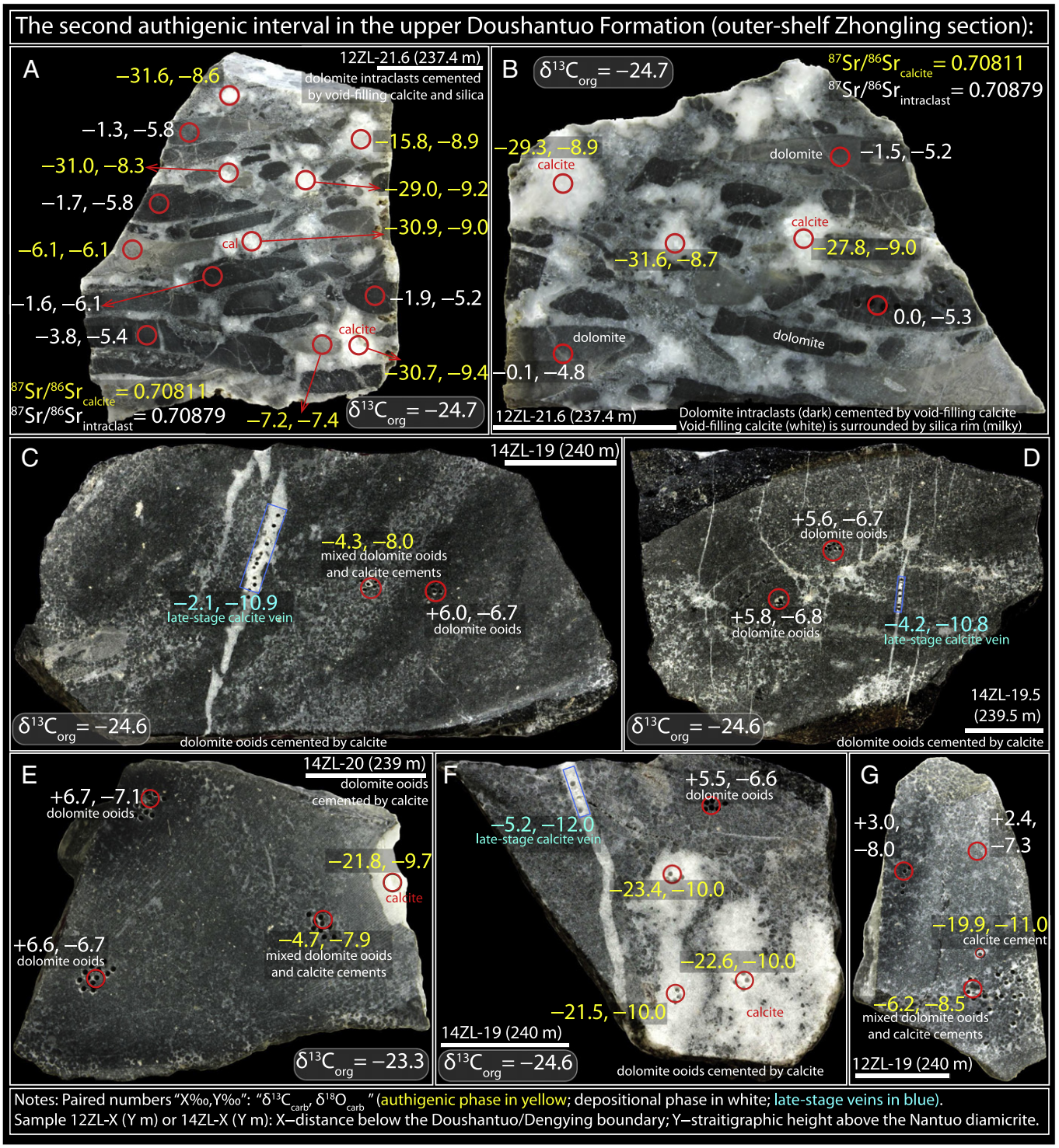

Fig. 6. Paired carbonate carbon and oxygen isotope data for micro-drilled spots in samples from the second stratigraphic interval of authigenic calcite in the Doushantuo Formation at the Zhongling section. See Fig. 8J for the stratigraphic position of the three intervals of authigenic calcite. Each pair of data shows $\delta^{13}C_{carb}$ (‰, VPDB) and $\delta^{18}O_{carb}$ (‰, VPDB), respectively. Organic carbon isotope ($\delta^{13}C_{org}$, VPDB) data of bulk acidified residues are also given for each sample. All scale bars are 2 cm long. Sample names were presented together with the scale bars. Stratigraphic height above the Marinoan (Nantuo) diamictite for each sample is provided in parentheses after each sample name. Yellow, white, and blue labels represent authigenic calcite phases, depositional phases, and late-stage veins, respectively. $^{87}Sr/^{86}Sr$ values are also shown for selected spots and samples when available.

pyrite and carbonate-associated sulfate (CAS) analyses at Jiulongwan record parallel negative trends from 0‰ to −20‰, and from +20‰ to 0‰, respectively, in the EN3 interval (Fig. 8D) (McFadden et al., 2008). However, at the Zhongling section, $\delta^{34}S$ values of pyrite and CAS remain invariant at around +20‰ and +40‰, respectively (Fig. 8M). At the intra-shelf Jiulongwan section, $^{87}Sr/^{86}Sr$ values are consistently low (ca. 0.7080) throughout most of the Doushantuo Formation, with a notable rise from 0.7080 up to 0.7090 during the EN3 interval (Fig. 8E) (Sawaki et al., 2010). In contrast, $^{87}Sr/^{86}Sr$ data measured from calcite/limestone phases of the Zhongling section remain

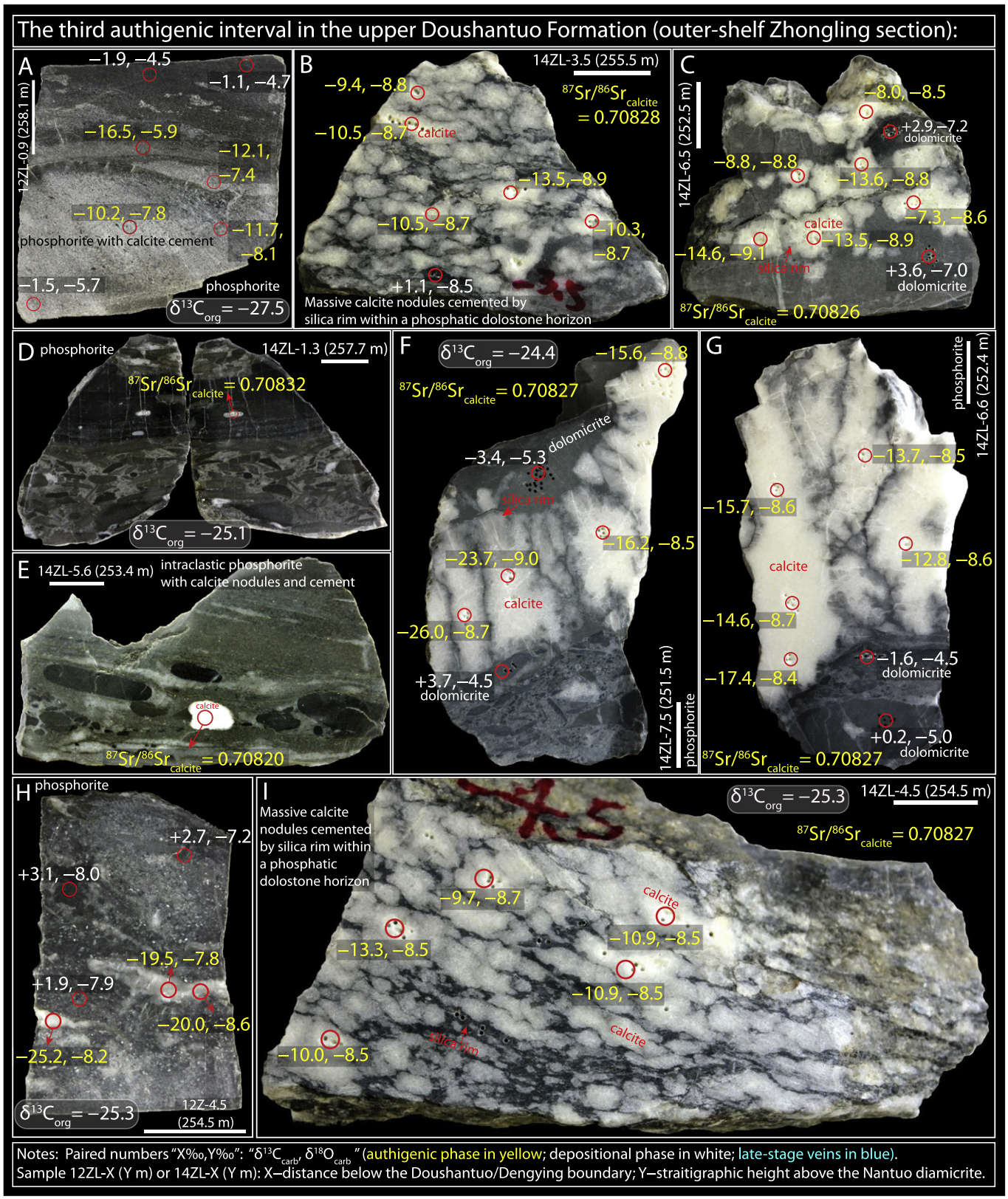

Fig. 7. Paired carbonate carbon and oxygen isotope data for micro-drilled spots in samples from the third stratigraphic interval of authigenic calcite in the Doushantuo Formation at the Zhongling section. See Fig. 8J for the stratigraphic position of the three intervals of authigenic calcite. Each pair of data shows $\delta^{13}C_{carb}$ (‰, VPDB) and $\delta^{18}O_{carb}$ (‰, VPDB), respectively. Organic carbon isotope ($\delta^{13}C_{org}$, VPDB) data of bulk acidified residues are also given for each sample. All scale bars are 2 cm long. Sample names were presented together with the scale bars. Stratigraphic height above the Marinoan (Nantuo) diamictite for each sample is provided in parentheses after each sample name. Yellow, white, and blue labels represent authigenic calcite phases, depositional phases, and late-stage veins, respectively. $^{87}Sr/^{86}Sr$ values are also shown for selected spots and samples when available.

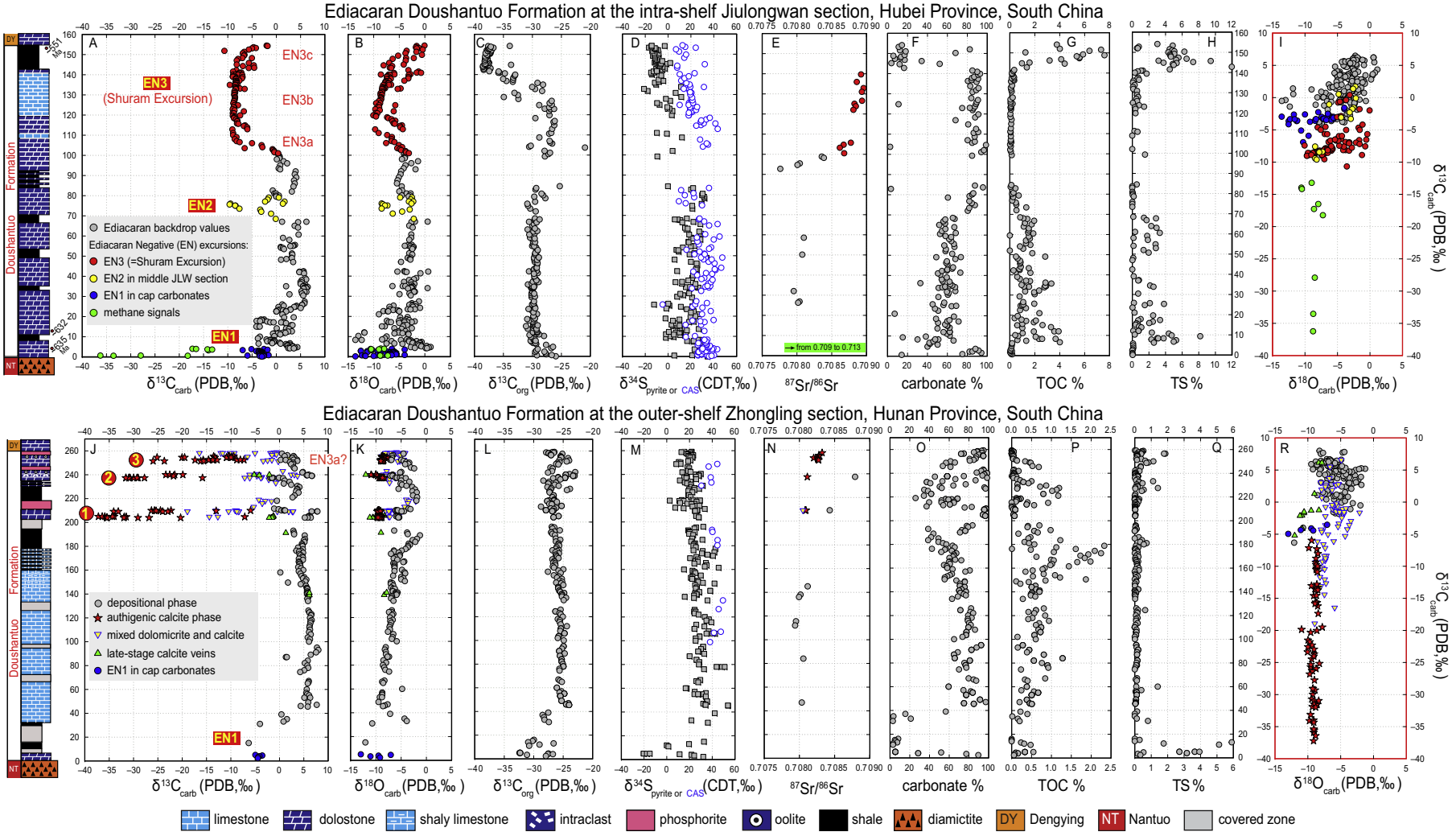

Fig. 8. Litho- and chemostratigraphic profiles for the Doushantuo Formation at the intra-shelf Jiulongwan section (A–I) and the outer-shelf Zhongling section (J–R). Texture- or phase-resolved geochemical data from micro-drilled spots are shown as different symbols. Cross plots of $\delta^{13}C_{carb}$ (‰, VPDB) vs. $\delta^{18}O_{carb}$ (‰, VPDB) are shown in I and R for the Jiulongwan section and the Zhongling section, respectively. The three intervals of authigenic calcite are identified in the upper 60 m of the Doushantuo Formation at the Zhongling section. Each interval is associated with a distinct phosphorite interval, suggesting potential linkage between authigenic carbonates and phosphorus cycle (Cui et al., 2016c). The third interval has been proposed to be correlative with the EN3a interval of the intra-shelf Jiulongwan section (Cui et al., 2015). Chemostratigraphic data of the Jiulongwan section are from Jiang et al. (2007); McFadden et al. (2008), and Sawaki et al. (2010). CAS = carbonate associated sulfate (shown as blue circles in D and M), EN = Ediacaran negative excursion, TOC=total organic carbon, TS=total sulfur in acidified residues. $\delta^{13}C_{carb}$ and $\delta^{18}O_{carb}$ data in authigenic phase of the Zhongling section are new, with $\delta^{34}S_{pyrite}$, $\delta^{13}C_{org}$ and $^{87}Sr/^{86}Sr$ data published in Cui et al. (2015). A complete dataset for the Zhongling section is included in the online supplementary material.

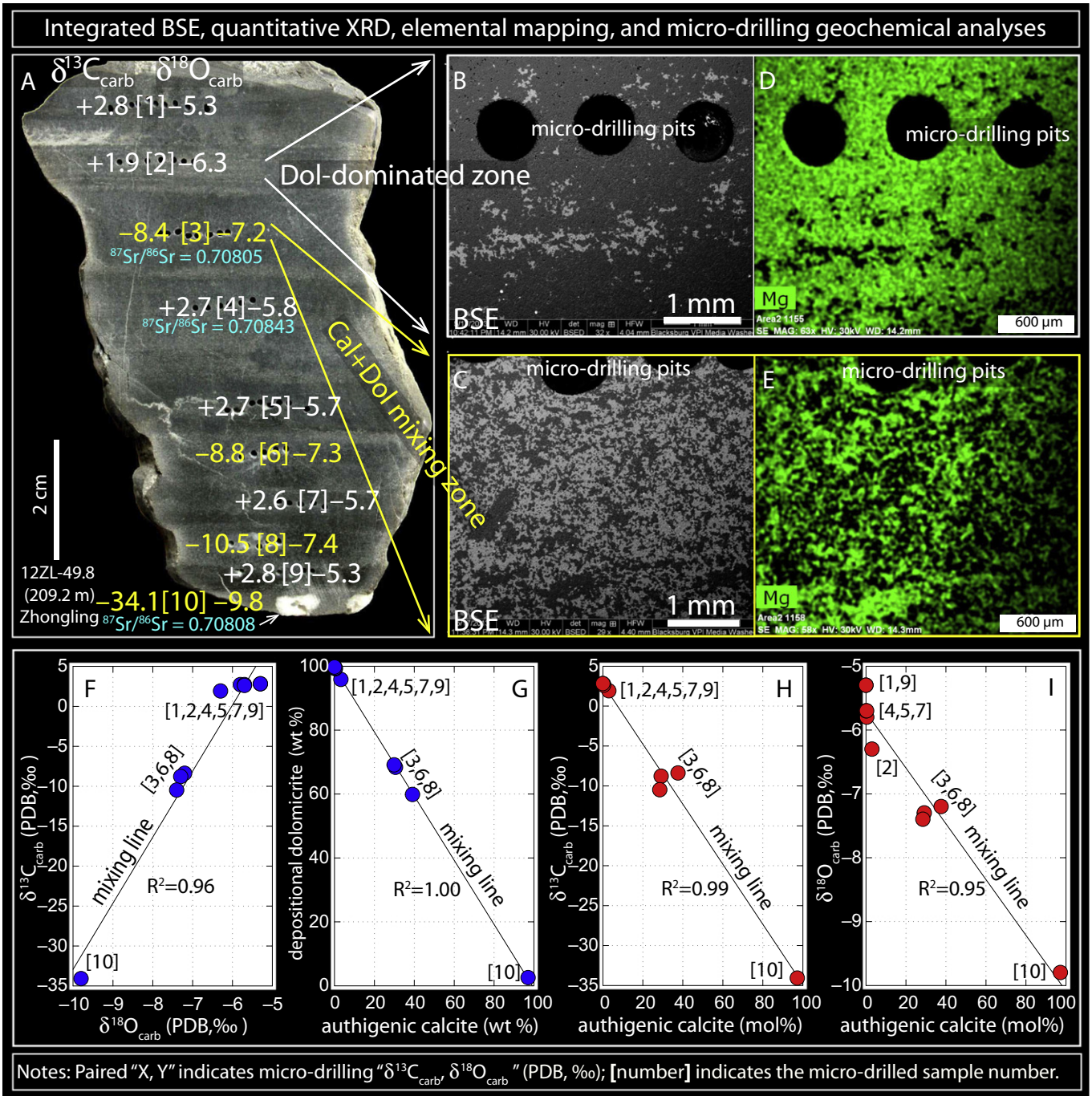

Fig. 9. Backscattered electron (BSE) images and quantitative X-ray powder diffraction (XRD) of a fine-grained dolostone sample (12ZL–49.8) from the Doushantuo Formation at the Zhongling section. The stratigraphic height for this sample is 209.2 m. (A) $\delta^{13}C_{carb}$ (‰, VPDB) and $\delta^{18}O_{carb}$ (‰, VPDB) values are shown for ten micro-drilled layers, including a small authigenic calcite nodule at the bottom. $^{87}Sr/^{86}Sr$ data are also shown when available. $^{87}Sr/^{86}Sr$ composition of dolomicrite-rich layer is slightly higher than calcite-dominated spots. (B, C) BSE images reveals that carbonate layer with positive $\delta^{13}C_{carb}$ is dolomicrite rich, while carbonate layer with negative $\delta^{13}C_{carb}$ is calcite rich. Dolomite in dark color, whereas calcite in light color. (D, E) Mg elemental maps of two micro-drilled samples marked as [2] and [3] in A, showing a dolomite-dominated layer and a mixed dolomicrite-calcite layer, respectively. Calcite in dark black color, whereas dolomite in bright green color. (F, G) Cross plots of isotopic compositions and mineralogical proportions (determined from quantitative XRD analysis) of the ten micro-drilled samples showing a mixing line between a dolomicrite end member and an authigenic calcite end member. (H, I) Cross plots between isotope and mineralogical compositions, showing that the degree of ^{13}C and ^{18}O depletion values is directly correlated to the percentage of authigenic calcite in each micro-sample. All data can be found in the online supplementary material.

steady at ca. 0.7080 in most of the section except for a slight rise to 0.7083 in the uppermost 10 m (Fig. 8N).

4.3. Co-variation of carbonate $\delta^{13}C$ and $\delta^{18}O$

Pervasively fine-grained carbonates with alternating calcite and dolomite-rich laminations from the upper Doushantuo Formation show strong heterogeneity of $\delta^{13}C_{carb}$ and $\delta^{18}O_{carb}$ on a centimeter-scale (Figs. 5–7, 9). For example, specimen 12ZL–49.8 (Fig. 9) – which has a grain size typical of most Ediacaran carbonates, including those deposited during the Shuram Excursion – reveals different proportional abundances of fine-grained dolomicrite and authigenic calcite in alternating sedimentary layers (Fig. 9B–E). The $\delta^{13}C_{carb}$ and $\delta^{18}O_{carb}$ data from each layer fall onto a well-correlated

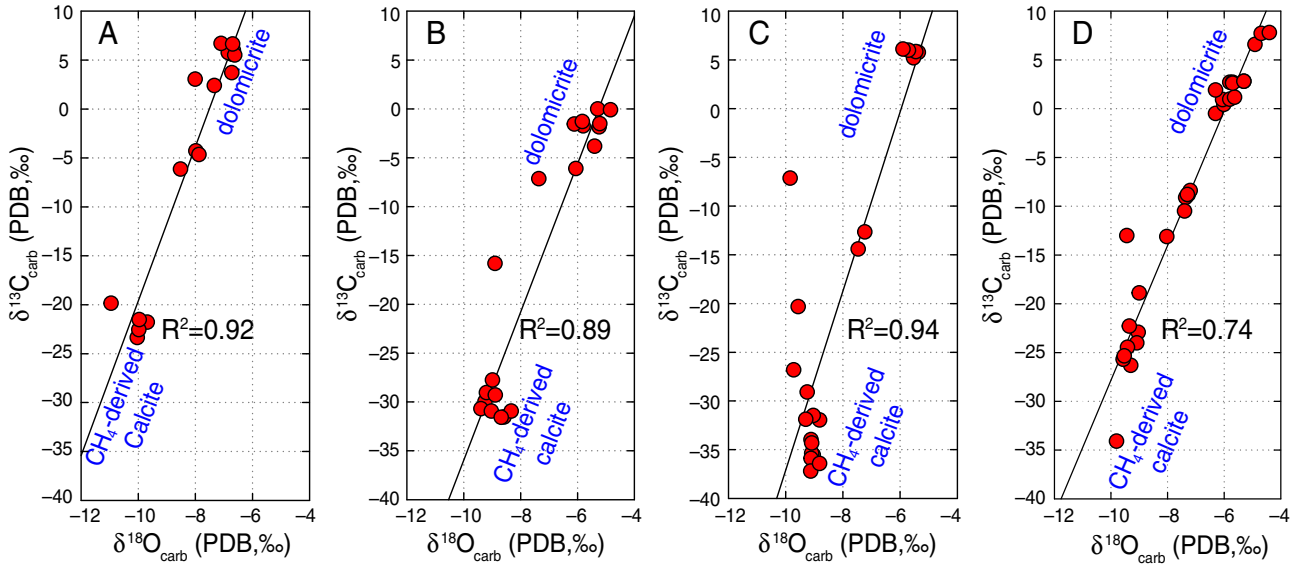

Fig. 10. Carbonate $\delta^{13}C$–$\delta^{18}O$ cross plots for different horizons in the upper 60 m of the Doushantuo Formation at the Zhongling section. Stratigraphically nearby samples are combined for the $\delta^{13}C$–$\delta^{18}O$ cross plots. (A) $\delta^{13}C$–$\delta^{18}O$ cross plots of oolitic dolostone with authigenic calcite cement at the stratigraphic height of ~240 m. Plotted data are measured from samples 12ZL-19,14ZL-19, 14ZL-19.5 and 14ZL-20; (B) $\delta^{13}C$–$\delta^{18}O$ cross plots of intraclastic dolostone with authigenic calcite cement at the stratigraphic height of 237.4 m. Plotted data are measured from sample 12ZL-21.6; (C) $\delta^{13}C$–$\delta^{18}O$ cross plots of interbedded dolomicrite layer and calcite layer at the stratigraphic height of ~210 m. Plotted data are measured from samples 14ZL-49,14ZL-49.2, 14ZL-49.8 and 12ZL-49.8; (D) $\delta^{13}C$–$\delta^{18}O$ cross plots of interbedded dolomicrite layer and calcite layer at the stratigraphic height of ~205 m. Plotted data are measured from samples 14ZL-53.5,14ZL-54, 14ZL-54.3 and14ZL-55.

mixing line (Fig. 9F) with one end member represented by the depositional dolomicrite phase ($\delta^{13}C_{carb}$ = ca. +3‰ and $\delta^{18}O_{carb}$ = ca. −5‰), and the other by the authigenic calcite phase ($\delta^{13}C_{carb}$ = ca. −34‰ and $\delta^{18}O_{carb}$ = ca. −10‰). XRD analyses of each layer were employed to quantify the abundance of depositional dolomicrite and authigenic calcite (Fig. S2, Table S4). We found that the magnitude of ^{13}C- and ^{18}O-depletion in each layer is strongly dependent on the relative abundance of authigenic calcite (Fig. 9F–I). Notably, the $\delta^{13}C_{carb}$ data range widely over 40‰ (from ca. +3‰ to −34‰), while $\delta^{18}O_{carb}$ data have a relatively narrow range (from ca. −5‰ to −10‰) in this sample. Similar mineralogical and isotopic systematics were noted in additional samples from different horizons in the Zhongling section (Fig. 10).

5. Discussion

5.1. An early authigenic origin for the ^{13}C-depleted calcite

5.1.1. Integrated sedimentological, petrographic, and geochemical evidence

Based on our detailed sedimentological, petrographic and geochemical analyses, we interpret the calcite nodules and cements from the upper Doushantuo Formation at Zhongling as early authigenic in origin having formed in unconsolidated sediments at or near the seafloor. At Zhongling, the preservation of authigenic calcite in nodules, cements, and fine-grained micrite intimately mixed with dolomicrite is associated with the three bedded phosphatic horizons (Fig. 2G–J). Due to preferentially weathering of calcite, weathered surfaces reveal an alternation of micrite- and dolomicrite-dominated laminations (Fig. 2G). No visible change in lithology or porosity was found within the phosphorite or dolostone horizons, nor did we observe any late-stage karst or metamorphic features that would otherwise suggest very late growth and preservation of the nodules.

In contrast to the calcite nodules and cements, the late-stage calcite veins are not strongly depleted in ^{13}C (most have $\delta^{13}C$ values > −5‰; Figs. S1D—F, 5B, F, H, 6C, D, F), but are notably more depleted in ^{18}O (Fig. 8K). The carbon and oxygen isotope contrast between bed-cutting calcite veins and the horizontally aligned calcite nodules suggests that the two calcitic textures were not precipitated from the same fluids, and that the late-stage veins likely developed from hydrothermal waters during deep burial.

Further support for an early authigenic origin of the ^{13}C-depleted calcite nodules and cements comes from their $^{87}Sr/^{86}Sr$ compositions and elemental abundances. Within each single sample, $^{87}Sr/^{86}Sr$ of dark-colored dolomitic phases (ranging from 0.7080 to 0.7088) are typically slightly more radiogenic than white-colored calcite phases (ranging from 0.7080 to 0.7083). This is the likely consequence of Sr loss during dolomitization and the addition of ^{87}Sr from ^{87}Rb decay in admixed clay minerals. On the other hand, the compositions of the calcite phases are remarkably consistent with contemporaneous Ediacaran seawater values recorded globally (Burns et al., 1994; Melezhik et al., 2009; Sawaki et al., 2010; Cui et al., 2015; Xiao et al., 2016), including bedded limestones lower in the Doushantuo Formation (Fig. 8N). Thus, the calcite nodules and cements are likely to more accurately reflect seawater Sr isotope compositions than the dolomites and phosphorites in which they are hosted. Elemental analyses for selected samples further indicate that calcite phases have much higher Sr concentration and much lower Fe, Mn, and Rb concentration when compared with dolomite matrices (Table S3), supporting their early authigenic origin. Similarly cathodoluminescence (CL) imaging of our samples show very dull color for the authigenic calcite nodules (Fig. 4I), which is consistent with an early diagenetic origin.

5.1.2. Comparison with methane-derived authigenic carbonates in cap carbonates

Similar to the calcite nodules and cements we have identified from the uppermost Doushantuo Formation, calcite with strong ^{13}C depletion also occurs as discrete textures in the cap dolostone at the base of the unit in the Yangtze Gorges area. On one hand, these isotopically anomalous calcites have been proposed as remnants of the oldest cold seep deposits, which formed during destabilization of methane hydrates in the aftermath of Marinoan glaciation (Jiang et al., 2003, 2006a, 2006b; Wang et al., 2008; Zhou et al., 2010, 2016). On the other, the same phases have been re-interpreted as the result of post-depositional hydrothermal events, based on petrographic observation (Lin et al., 2011), clumped isotope analyses (Bristow et al., 2011), and combined organic matter and clay mineral analysis (Derkowski et al., 2013).

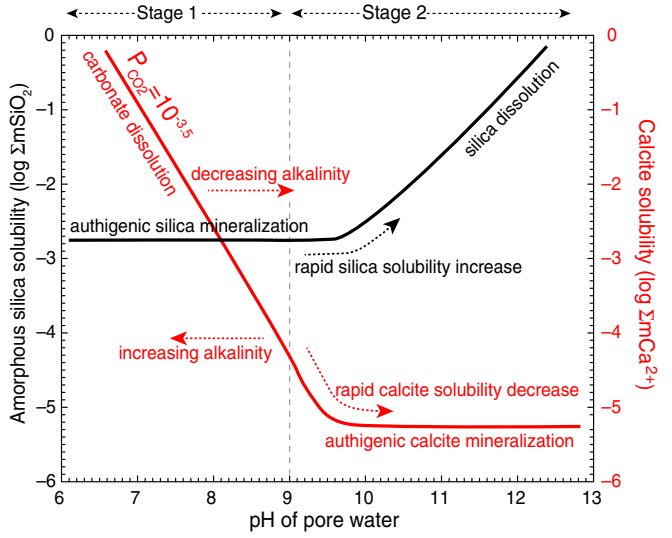

Fig. 11. Solubility of amorphous silica (left y-axis) and calcite (right y-axis) as a function of pH, modified from Figs. 6.6 and 7.7 of Langmuir et al. (1997) and Fig. S1 of Xiao et al. (2010). Calcite solubility calculated at 25 °C and 1 bar total pressure with an assumed $P_{CO2} = 10^{-3.5}$ bar. The growth of authigenic calcite and quartz could be described as a two-stage process in response to changes in pH. Stage 1 is characterized by the dissolution of pre-existing host carbonate and authigenic mineralization of quartz. Stage 2 is characterized by authigenic mineralization of calcite and partial replacement of quartz by calcite. See the main text for full discussion.

Notably, the $^{87}Sr/^{86}Sr$ ratios in the basal Doushantuo cap dolostone are highly radiogenic (up to ca. 0.7130) (Fig. 8E), and furthermore these phases are spectacularly enriched in Mn (over 20,000 ppm resulting in Mn/Sr up to 600) (Sawaki et al., 2010; Bristow et al., 2011; Huang et al., 2011). These observations suggest significant water-rock interaction after burial (Marshall, 1992; Jacobsen and Kaufman, 1999).

In contrast, the calcite nodules and cements discovered in this study from the upper Doushantuo Formation at Zhongling all preserve typical Ediacaran seawater $^{87}Sr/^{86}Sr$ values (ca. 0.7080), suggesting an early authigenic origin for these phases, which appear to have been in diffusive contact with a dominantly marine Sr source. Authigenic carbonates with seawater Sr signals are common in Modern marine sediments (e.g., Hovland et al., 1987; Aharon et al., 1997; Naehr et al., 2000; Greinert et al., 2001; Peckmann et al., 2001; Joseph et al., 2012). When marine sediments are still unconsolidated with free diffusion of Sr from seawater, authigenic carbonates will capture seawater Sr isotope compositions. The high concentration of Sr and low concentration of Mn, Fe and Rb in the Zhongling authigenic calcite phases is also in strong contrast with those from the basal Doushantuo cap carbonate, which supports our view that each has a unique origin.

In summary, sedimentological, petrographic, and geochemical observations of the isotopically-distinct calcite phases from the uppermost Doushantuo Formation at Zhongling support the view that they are early authigenic in origin. They appear not to be associated with post-lithification hydrothermal events (e.g., Bristow et al., 2011; Derkowski et al., 2013; Hohl et al., 2015). Thus, we interpret the bedded, fine grain-sized, phosphatic or dolomitized carbonates as depositional phases, and these textually- and isotopically-distinct calcite cements and nodules as syndepositional authigenic phases.

5.2. Mechanism for authigenic mineralization

In our view, the biogeochemical processes responsible for authigenic mineralization in the uppermost Doushantuo sediments prior to lithification are directly related to variations in the pH and alkalinity of pore waters due to microbial activity (Fig. 11) (Walter et al., 1993; Langmuir et al., 1997; Morse, 2003). Geochemical consideration of microbial sulfate reduction (Eq. 1), which is often coupled with the anaerobic oxidation of methane (Eq. 2), indicates that the onset of this metabolic activity initially lowers the pH, which would favor the dissolution of the pre-existing carbonates (Eq. 3) (Birnbaum and Wireman, 1984; Morse and Mackenzie, 1990; Walter and Burton, 1990; Walter et al., 1993; Morse, 2003; Meister, 2013), as well as the precipitation of authigenic silica (Eq. 4) (Stage 1 in Fig. 11). The production of sulfide would result in the formation of pyrite so long as ferrous iron were available in the sediments, and the observation of disseminated pyrite (Fig. 3H, I) is a testament to this microbial process.

$$SO_4^{2-} + 2CH_2O \rightarrow HS^- + 2HCO_3^- + H^+ \quad (1)$$

$$SO_4^{2-} + CH_4 \rightarrow HS^- + HCO_3^- + H_2O \quad (2)$$

$$CaCO_3 + H^+ \rightarrow Ca^{2+} + HCO_3^- \quad (3)$$

$$SiO_3^{2-} + H^+ \rightarrow SiO_2 + OH^- \quad (4)$$

As sulfate reduction progresses, however, the pH is stabilized and calcite saturation increases with the buildup of alkalinity (Morse and Mackenzie, 1990; Walter et al., 1993; Morse, 2003; Meister, 2013), especially if methane is the primary organic substrate (Moore et al., 2004) (Stage 2 in Fig. 11). As alkalinity in pore waters rises and becomes increasingly saturated, the concomitant rise in pH would favor the dissolution of pre-existing silica and authigenic precipitation of ^{13}C-depleted calcite (Eq. 5) (e.g., Berner, 1971; Ritger et al., 1987).

$$Ca^{2+} + CO_3^{2-} \rightarrow CaCO_3 \quad (5)$$

In light of the intimate association between authigenic calcite and the three phosphatic intervals, microbial iron reduction during the phosphorite formation, which is also known as the "Fe-P shuttle" (Muscente et al., 2015; Cui et al., 2016c), may have also played a role in the production of alkalinity and authigenic mineralization. Carbonate saturation would also increase during microbial iron reduction (Eq. 6) (Riedinger et al., 2014). Microbial reduction of FeOOH is a strong sink of H^+ that increases pore water pH and can promote carbonate precipitation (Coleman and Raiswell, 1995):

$$4FeOOH + CH_2O + 7H^+ \rightarrow 4Fe^{2+} + HCO_3^- + 6H_2O \quad (6)$$

In addition, abiological reduction of FeOOH by sulfide produced via microbial sulfate reduction (Eq. 7) may also consume acidity and promote authigenic carbonate formation:

$$2FeOOH + HS^- + 5H^+ \rightarrow 2Fe^{2+} + S^0 + 4H_2O \quad (7)$$

It is notable that disseminated and framboidal pyrite is widespread in the studied samples, and its authigenic formation may have been promoted by the coupling of sulfate and iron reduction by a consortium of micro-organisms. Ferrous iron in pore fluids could be produced by microbial iron reduction, and react with sulfide produced by microbial sulfate reduction to form authigenic pyrite (Eq. 8).

$$Fe^{2+} + HS^- \rightarrow FeS + H^+;\ FeS + S^0 \rightarrow FeS_2 \quad (8)$$

An integrated reaction combining microbial sulfate and iron reduction is summarized below (Eqs. 9, 10):

$$6CH_2O + 3SO_4^{2-} \rightarrow 6HCO_3^- + 3H_2S \quad (9)$$

$$2FeOOH + 3H_2S + S^0 \rightarrow 2FeS_2 + 4H_2O \quad (10)$$

In summary, well-preserved authigenic precipitates, including authigenic calcite nodules and cements, authigenic silica rim surrounding the calcite, and disseminated pyrite, recorded multiple stages of

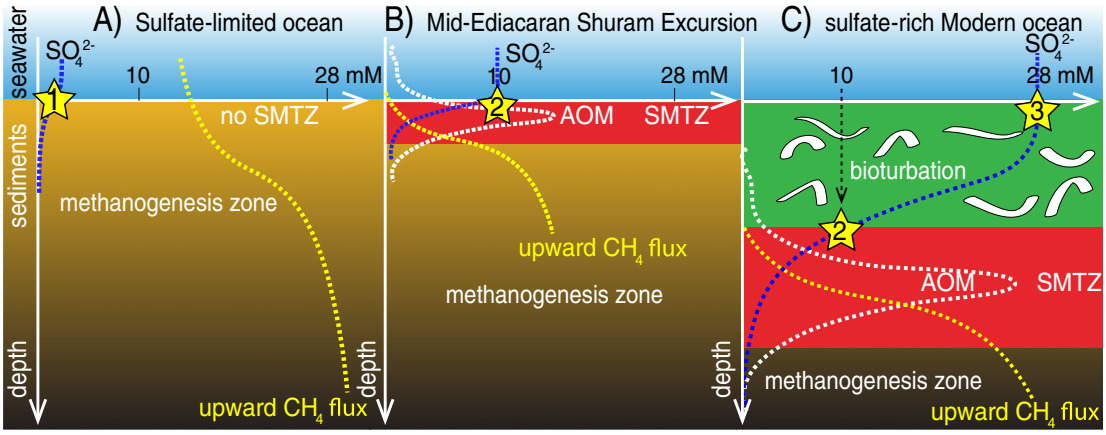

Fig. 12. Progressive deepening of a sulfate–methane transition zone (SMTZ) driven by increasing seawater sulfate concentrations. (A) A scenario lacking a SMTZ due to extremely low sulfate concentration in seawater for most of the Precambrian time. In this scenario, biogenic methane flux may have largely escaped out of the sediments into the water column and the atmosphere. (B) Based on the novel observation of authigenic calcite in this study, we propose that the SMTZ may be placed near the sediment–water interface in response to an increase in seawater sulfate concentration. (C) With the emergence of bioturbation and further increase in seawater sulfate concentration, the SMTZ in modern marine environments is driven deeper into the sediments. The evolution of the SMTZ is proposed to be closely linked to the seawater sulfate concentration through the Earth's history. The sulfate concentration was ca. 200 μM or less before 2.4 Ga (Habicht et al., 2002; Zhelezinskaia et al., 2014). After this, concentrations rose to values probably not exceeding 1 to 2 mM over the next 1.6 billion years or so (yellow star 1 in A) (Canfield and Farquhar, 2009). Based on the observation of modern marine sediments, anaerobic oxidation of methane (AOM) within SMTZ requires sulfate concentration in pore water to be <10 mM (yellow star 2 in C) (Jørgensen and Kasten, 2006). Projecting this threshold to scenario B, the formation of authigenic carbonates within a seafloor SMTZ requires seawater sulfate to be no more than ca. 10 mM (yellow star 2 in B). The sulfate concentration in the modern ocean is ca. 28 mM (yellow star 3 in C).

early authigenic mineral growth mediated by a consortium of microbes. This process is accompanied by varying pH conditions in pore water, and is controlled by the flux of sulfate, silicon, and iron from seawater through unconsolidated marine sediments.

5.3. Conceptual model for the $\delta^{13}C$ anomaly

5.3.1. Progressive deepening of the sulfate–methane transition zone

In the uppermost Doushantuo Formation at Zhongling, highly negative $\delta^{13}C$ values (as low as −37‰) of authigenic calcite suggest that the anaerobic oxidation of methane by microbial sulfate reduction occurred in pore waters within the sulfate–methane transition zone (SMTZ) (Fig. 12) (Jørgensen and Kasten, 2006; Xu, 2010). In modern marine environments rich in sulfate, the upward methane flux is exhausted in the SMTZ through sulfate reduction (Jørgensen, 1982), except in localized cold seeps where excess methane can escape to seawater (Greinert et al., 2001; Haeckel et al., 2004; Campbell, 2006; Suess, 2014). The SMTZ denotes a microbial transition within an anoxic sediment column where pore water sulfate and methane concentration profiles intersect at non-detectable levels (Fig. 12C). The depth of SMTZ depends on the relative size of upward methane flux from the depth and the downward diffusion of sulfate from overlying seawater (Borowski et al., 1996, 1999).

In light of the observation in this study, we propose that the anomalous negative carbon isotope signals in the uppermost Doushantuo Formation may have formed from syndepositional authigenesis in a shallow SMTZ. To allow for the progressive deposition of early authigenic carbonates, we hypothesize that the inferred SMTZ was likely to be immediately below the sediment–water interface (Fig. 12B) (Greene et al., 2012; Husson et al., 2015b; Meister, 2015; Saitoh et al., 2015). We realize that similar analogues in modern marine environments are lacking, but insofar as redox conditions in terminal Proterozoic oceans were likely to be quite different from those of the modern, a non-actualistic approach (e.g., Catling et al., 2007; Grotzinger et al., 2011; Schrag et al., 2013; Meister, 2015; Zhou et al., 2015) is required in order to reconcile the observations described above.

In modern marine sediments, the depth of SMTZ may vary strongly among different localities, ranging from centimeter to hundreds of meters in scale depending on the water depth, organic flux, and the balance between the downward flux of sulfate and the upward flux of methane (Borowski et al., 1996, 1999). Generally, the SMTZ is shallow where the methane flux dominates (e.g., above localized gas hydrate reservoirs), and is deeper where diffusion of seawater sulfate dominates the system. Insofar as marine sulfate concentration progressively increased in the Neoproterozoic (Halverson and Hurtgen, 2007; Canfield and Farquhar, 2009; Cui et al., 2016b), the position of the SMTZ in marine sediments may have been initially located near the sediment–water interface, and then moved deeper over time in response to the increasing flux of the oxidant (e.g., sulfate or iron oxide) as the result of elevated oxidative weathering or an increase in bioturbation.

With the emergence of bioturbation in the terminal Ediacaran and Cambrian periods (Bottjer et al., 2000; Carbone and Narbonne, 2014), ventilation of the deep ocean (Logan et al., 1995; Butterfield, 2009, 2011; Lenton et al., 2014; Chen et al., 2015), and a larger seawater sulfate pool (Halverson and Hurtgen, 2007; Canfield and Farquhar, 2009; Cui et al., 2016b), the Phanerozoic SMTZ would have been progressively deeper compared with the SMTZ in Precambrian time (Fig. 12C) (see Wright and Cherns, 2016 for a Phanerozoic analogue). Conversely, during most of the Precambrian, due to the very low sulfate concentration in the ocean, the SMTZ may not exist in marine sediments, and the biogenic methane flux may have directly escaped into the atmosphere (e.g., Halverson et al., 2002; Pavlov et al., 2003; Catling et al., 2007; Ader et al., 2009; Bristow and Grotzinger, 2013; Li et al., 2015; Shen et al., 2016) (Fig. 12A).

Our conceptual model offers an attractive scheme to explain the uniqueness of the Shuram Excursion in Earth's history. The stratigraphic expression of the Shuram Excursion may have been triggered by a mid-Ediacaran development of a sulfate-methane transition zone near the seafloor. Continuous syndeposition of early authigenic carbonates in this shallow redox zone led to full expression of the Shuram Excursions in stratigraphic records of continental margins where sulfate concentration increased to threshold levels (ca. 10 mM, see the next section for quantitative constraints) in response to the Neoproterozoic Oxygenation Event. Overall low sulfate condition during most of the Precambrian may have significantly inhibited the development of the sulfate-methane transition zone (Catling et al., 2007), resulting in the absence of Shuram-like excursions. Conversely, too high concentration (>10 mM) of seawater sulfate and the emergence of bioturbation during most of the Phanerozoic may have played a role in driving the sulfate-methane transition zone into much deeper depths, consequently

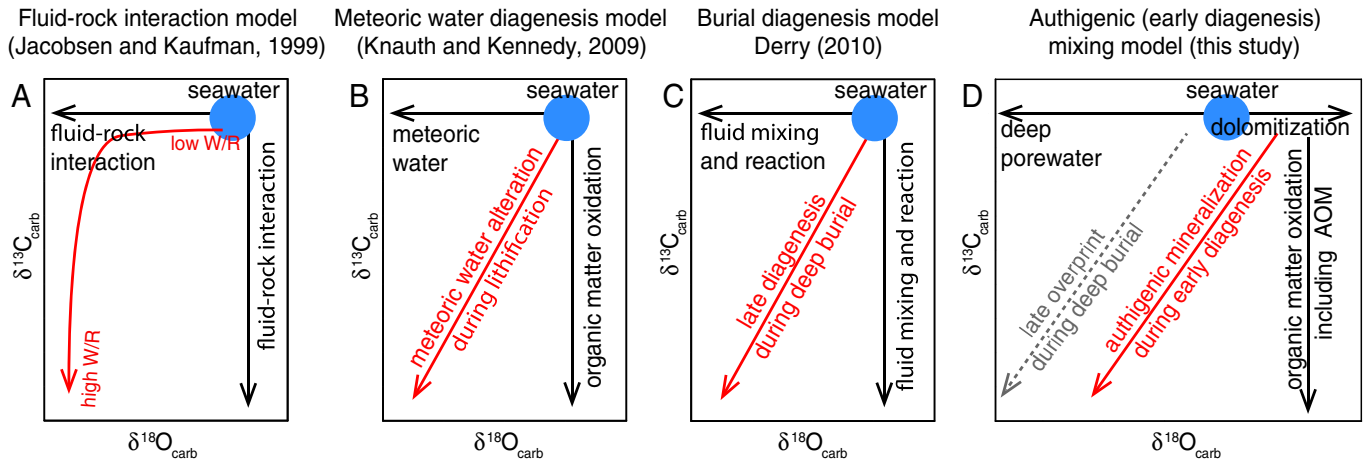

Fig. 13. Different models for the interpretation of $\delta^{13}C_{carb}$–$\delta^{18}O_{carb}$ co-variation in the late Precambrian carbonate strata. (A) $\delta^{13}C_{carb}$ and $\delta^{18}O_{carb}$ model proposed by Jacobsen and Kaufman (1999). This model defines a hyperbolic curve with increasing fluid-rock interaction. $\delta^{18}O_{carb}$ is more prone to diagenetic overprint compared with $\delta^{13}C_{carb}$. (B) Meteoric alteration model proposed by Knauth and Kennedy (2009). Based on this model, *assuming* the existence of considerable terrestrial biomass, Knauth and Kennedy (2009) proposed a global greening event during late Precambrian. (C) Burial diagenesis model proposed by Derry (2010a). Based on this model, Derry (2010a) argued that the global Shuram Excursion results from burial diagenesis, and thus lacks paleoclimatic significance. (D) Authigenic mixing model proposed in this study. Based on novel data revealed in this study, we propose that the tight $\delta^{13}C_{carb}$–$\delta^{18}O_{carb}$ correlation in the uppermost Doushantuo Formation, and potentially also in the global Shuram Excursion, results from progressive authigenic mineralization of primary marine carbonates during very early diagenesis. Late diagenesis during deep burial may have led the overall $\delta^{18}O_{carb}$ compositions to more negative values. See the main text for detailed discussion. AOM = Anaerobic Oxidation of Methane.

switched the depositional pattern of authigenic carbonates from syn-deposition to post-deposition. In summary, the uniqueness of the Shuram Excursion in Earth's history may result from an overall irreversible increase of seawater sulfate concentration (due to oxidative weathering associated with orogeny, reflected in the rise of seawater $^{87}Sr/^{86}Sr$ compositions, and coupled with the buildup of oxygen in the atmosphere), and an enhanced activity of bioturbation during the Phanerozoic. These two factors may have influenced the depth of the sulfate-methane transition zone where syn-deposition or post-deposition of authigenic carbonates occurred.

5.3.2. Quantitative constraint on seawater sulfate concentration

If our conceptual model of shallow authigenesis holds true for the middle Ediacaran Shuram Excursion, quantitative constraint on seawater sulfate concentration might be possible (Fig. 12). In modern environment with sulfate concentration at ca. 28 mM (Star 3 in Fig. 12C), methanogens are typically outcompeted for substrates (e.g. lactate and acetate) by sulfate reducers, so the SMTZ is only developed when pore-water sulfate concentration is lower than ca. 10 mM within the sediments (Jørgensen and Kasten, 2006) (Star 2 in Fig. 12C). Extrapolating this sulfate threshold to a shallow SMTZ just beneath the sediment–water interface (Star 2 in Fig. 12B), the seawater sulfate concentration should have been no >10 mM if authigenesis occurs immediately above the sediment–water interface (evidenced by seafloor crystal fans in some localities; Pruss et al., 2008; Hall et al., 2013; Loyd et al., 2013). At Zhongling, the sulfate concentration in seawater might have been slightly higher than 10 mM to allow the growth of authigenic nodules in SMTZ within shallow marine sediments. This estimate is consistent with a recent model based on time-series sulfur isotope variation, which suggests that oceanic sulfate concentration was low (<5 mM) in the aftermath of the Marinoan ice age (ca. 635 Ma), but rose sharply (to ca. 10 mM) near the Ediacaran–Cambrian boundary (Algeo et al., 2015).

5.4. Origin of co-varying carbon and oxygen isotopes

5.4.1. Published models for $\delta^{13}C_{carb}$ and $\delta^{18}O_{carb}$ covariation

The recognition of alternating laminations dominated by micrite and dolomicrite in outcrop allowed for petrographic and isotopic tests of the authigenic hypothesis, and a possible connection to the Shuram Excursion. Several hypotheses have been proposed to interpret positive correlations between $\delta^{13}C_{carb}$ and $\delta^{18}O_{carb}$ (Fig. 13). The progressive increase of fluid-rock interaction during carbonate diagenesis could cause different degrees of depletion in ^{13}C and ^{18}O (Jacobsen and Kaufman, 1999). Based on simple box modeling, $\delta^{18}O_{carb}$ could be reset more easily (i.e., less rock-buffered) than $\delta^{13}C_{carb}$ compositions, thereby forming a hyperbolic relationship (Fig. 13A). This mechanism may be true for some sample sets (e.g., Lohmann, 1988; Bishop et al., 2014), but does not explain the linear relationship of $\delta^{13}C_{carb}$ and $\delta^{18}O_{carb}$ revealed in this study (Figs. 9, 10).

Based on the positive $\delta^{13}C_{carb}$–$\delta^{18}O_{carb}$ correlations in modern marine sediments, which results from meteoric water alteration (e.g., Gross and Tracey, 1966; Quinn, 1991; Swart and Kennedy, 2012; Oehlert and Swart, 2014), Knauth and Kennedy (2009) interpreted similar observations in Ediacaran sedimentary rocks as a result of globally-distributed diagenetic event associated with the flushing of meteoric waters depleted in both ^{13}C and ^{18}O through shallow marine sediments. This model assumes a widespread terrestrial biosphere during the Ediacaran Period (Fig. 13B), and has been widely adopted as a universal criterion for diagenetic evaluation in chemostratigraphic studies (e.g., Xiao et al., 2012; Lu et al., 2013; Tahata et al., 2013; Osburn et al., 2015; Schobben et al., 2016).

Alternatively, the isotopic covariation has also been interpreted as resulting from a series of fluid-rock interactions associated with deep burial long after deposition (Fig. 13C) (Derry, 2010a, 2010b). Contrary to the Jacobsen and Kaufman (1999) model, which describes only "passive" trace element or isotopic exchange, but does not include any chemical reactions between fluid and rock, Derry (2010a) used another approach. It takes an initial system containing fluid and minerals in equilibrium at a given temperature, and then this system reacts with addition of a new infiltrating "reactant" fluid of a different composition at progressively higher water/rock ratio. Thus mineral and fluid compositions are continuously re-calculated from equilibrium relationships as the system composition evolves. This approach may better reflect the pore water condition as the burial depth becomes progressively deeper. Indeed, with this revised approach, the linear relationship in $\delta^{13}C_{carb}$ vs. $\delta^{18}O_{carb}$ could be well explained by this model.

These hypotheses, however, are inconsistent with the excellent preservation of fine-grained and texturally complex carbonates with geochemically-distinct and mineralogically-dependent heterogeneity.

For example, if meteoric water percolated the strata, we would expect pervasive alteration, as opposed to the preservation of well aligned calcite nodules surrounded by distinct quartz rim. Late diagenesis controlled by sediment porosity and permeability could indeed cause strong heterogeneity (e.g., Moore, 1989, 2004; Ahr, 2011; Morad et al., 2013), but this scenario can be ruled out considering the pervasively fine grained dolomicrite host carbonates in the upper Doushantuo Formation. Moreover, both meteoric water alteration and deep burial diagenesis could not sufficiently explain the extremely negative $\delta^{13}C_{carb}$ and typical Ediacaran seawater $^{87}Sr/^{86}Sr$ signals exclusively preserved in the calcite nodules. Thus, we disfavor these diagenetic models as explanations for the covariance in $\delta^{13}C_{carb}$ and $\delta^{18}O_{carb}$ revealed in the Zhongling carbonates.

5.4.2. An authigenic mixing model

In light of the sedimentological, petrographic, and isotopic observation in the uppermost Doushantuo Formation (Figs. 2–8), we propose that the strong $\delta^{13}C_{carb}$–$\delta^{18}O_{carb}$ correlation likely resulted from variations in the degree of authigenic carbonate mineralization (Fig. 13D). BSE images reveal sedimentary layers of fine-grained dolomicrite with variable amount of authigenic calcite (Fig. 9), resulting in $\delta^{13}C_{carb}$ and $\delta^{18}O_{carb}$ compositions that fall on a mixing line between end-member compositions. XRD analyses of each layer were employed to quantify the relative abundance of depositional dolomicrite and authigenic calcite, and we found that the magnitude of ^{13}C- and ^{18}O-depletion is strongly dependent on the relative abundance of authigenic calcite (Fig. 9H, I).

The differences in $\delta^{18}O_{carb}$ compositions of the calcite and dolomicrite end members in our samples from Zhongling samples are on the order of ca. 5‰, with calcite being systematically depleted in ^{18}O (Figs. 8K, 9, 10). This may reflect an isotope effect between calcite and dolomite during precipitation or dolomitization. Both experimental studies (Northrop and Clayton, 1966; O'Neil and Epstein, 1966; Sheppard and Schwarcz, 1970; Horita, 2014) and natural samples (Degens and Epstein, 1964; Gross and Tracey, 1966; Sass et al., 1991; Metzger and Fike, 2013; Li et al., 2016) have shown ca. +5‰ enrichment of ^{18}O in co-existing dolomite relative to calcite forming from the same solution. This isotopic effect may be responsible for the $\delta^{18}O_{carb}$ variation during the mixing between authigenic calcite and depositional dolomite in the studied samples.

5.4.3. An oxygen isotope enigma

It should be noted that the $\delta^{18}O_{carb}$ compositions in both depositional phase and authigenic phase are more negative than modern seawater values (Rohling, 2007). To interpret the $\delta^{18}O_{carb}$ behavior in the studied rocks, the Ediacaran seawater $\delta^{18}O$ composition would need to be known *a priori*, but this remains a matter of ongoing debate. On one hand, lower seawater $\delta^{18}O$ (ca. −7‰ PDB) has been proposed for the Neoproterozoic ocean (Veizer et al., 1997, 1999; Kasting et al., 2006; Jaffrés et al., 2007), but on the other hand it has also been argued that the seawater $\delta^{18}O$ composition through Earth history may remain largely constant (Muehlenbachs and Clayton, 1976; Muehlenbachs, 1998; Knauth, 2005).

If the Ediacaran seawater $\delta^{18}O$ is consistent with the modern seawater value, then the question becomes: what mechanism leads to the decrease of $\delta^{18}O$ data in the Precambrian carbonates, particularly in these authigenic calcite revealed in this study? In both the meteoric water alteration model (Fig. 13B; Knauth and Kennedy, 2009) and the burial diagenesis model (Fig. 13C; Derry, 2010a), the authors assumed that the Ediacaran seawater $\delta^{18}O$ was indistinguishable from the modern and they therefore proposed diagenetic alteration as the only mechanism for the decrease of Precambrian $\delta^{18}O$ carbonate values. However, this fundamental assumption should be treated with caution given the controversial understanding of deep time $\delta^{18}O$ evolution in the ocean (Arthur, 2009).

Alternatively, if the Ediacaran seawater $\delta^{18}O$ composition is indeed much lower (e.g., −7‰; Kasting et al., 2006; Jaffrés et al., 2007) than the modern seawater value, then the question becomes: what mechanism leads the $\delta^{18}O$ variability in mineralogically different carbonate phases towards opposite directions on a centimeter scale? As revealed from the uppermost Doushantuo Formation at Zhongling, the depositional phase (i.e., pervasively fine-grained dolomicrite) has generally higher $\delta^{18}O$ values, while the early authigenic phase (i.e., methane-derived calcite) have generally lower $\delta^{18}O$ values.

Variation in the $\delta^{18}O$ of seawater or pore water during early diagenesis can result from local evaporation (Li and Ku, 1997; Kah, 2000; Gomez et al., 2014; Horton et al., 2015), gas hydrate formation (Davidson et al., 1983; Teichert et al., 2005; Kennedy et al., 2008; Nyman and Nelson, 2011), or glacial ice buildup or melting (Zhao and Zheng, 2010; Peng et al., 2013; Wang et al., 2014; Zhao and Zheng, 2015). Progressive changing in these environmental factors, or end-member mixing among different reservoirs influenced by these factors could indeed cause potential correlation in $\delta^{13}C_{carb}$ vs. $\delta^{18}O_{carb}$ (e.g., Li and Ku, 1997; Horton et al., 2015; Mishra et al., 2015). However, to link these potential mechanisms to the uppermost Doushantuo Formation requires a comprehensive evaluation based on integrated sedimentological, petrographic, and geochemical observations. At present, there is still no clear evidence for any of these mechanisms. Laboratory experiments also reveal that solution pH, alkalinity (Spero et al., 1997), carbonate precipitation rate (Watkins et al., 2014), and salinity (Adkins et al., 2002) could also influence the $\delta^{18}O$ compositions. However, these effects are modest, only 1–2‰ at most.

The effect of early authigenesis on pore water $\delta^{18}O$ compositions in natural marine sediments remains largely unknown. Studies reveal that $\delta^{18}O$ compositions of early authigenic calcite are typically more depleted in ^{18}O than co-existing host carbonates (e.g., Sass et al., 1991; Mozley and Burns, 1993; Melezhik et al., 2007). The detailed mechanism remains unclear, but may be associated with either potential mixing of more ^{18}O-depleted sources (e.g., pore water sulfate, meteoric water, glacial meltwater) during very early diagenesis, or *in situ* precipitation of ^{18}O-enriched sinks (e.g., gas hydrate associated clathrate, clay minerals) within sediments. Currently, there is still no data available to test these hypotheses.

Clumped isotope analyses of other time-equivalent strata (Bergmann, 2013; Loyd et al., 2015) suggest different degrees of diagenetic overprint by increasing fluid-rock interaction during deep burial. This may partially support the late diagenesis model proposed by Derry (2010a), but cannot be reconciled with a variety of sedimentological observations that strongly point to an early authigenic origin (Grotzinger et al., 2011). Thus, on one hand we recognize potential diagenetic overprint in our samples (and probably in most carbonate samples of Precambrian age); on the other hand, we regard different degrees of authigenic mineralization during very early diagenesis as the main reason for the tight $\delta^{13}C_{carb}$–$\delta^{18}O_{carb}$ correlation (Fig. 13D).

In summary, detailed sedimentological, geochemical, and petrographic investigations suggest that the tight $\delta^{13}C_{carb}$–$\delta^{18}O_{carb}$ correlation results from progressive mixing of authigenic calcite in depositional dolomite (Figs. 9, 10). The ca. 5‰ range in $\delta^{18}O_{carb}$ that is generally lower than normal seawater values likely reflects a superimposed effect by both calcite-dolomite fractionation and burial diagenesis as evidenced by clumped isotopes (Loyd et al., 2015). If true, our data support the view that $\delta^{18}O_{carb}$ is less rock-buffered and more sensitive to diagenetic alteration than $\delta^{13}C$ and $^{87}Sr/^{86}Sr$ (Lohmann, 1988; Banner and Hanson, 1990; Jacobsen and Kaufman, 1999; Bishop et al., 2014; Loyd et al., 2015). However, to better interpret the overall negative $\delta^{18}O_{carb}$ compositions in both depositional and authigenic phases requires a better understanding of the Ediacaran seawater $\delta^{18}O$ compositions, as well as the detailed knowledge about the effect of authigenesis on pore water $\delta^{18}O$ compositions.

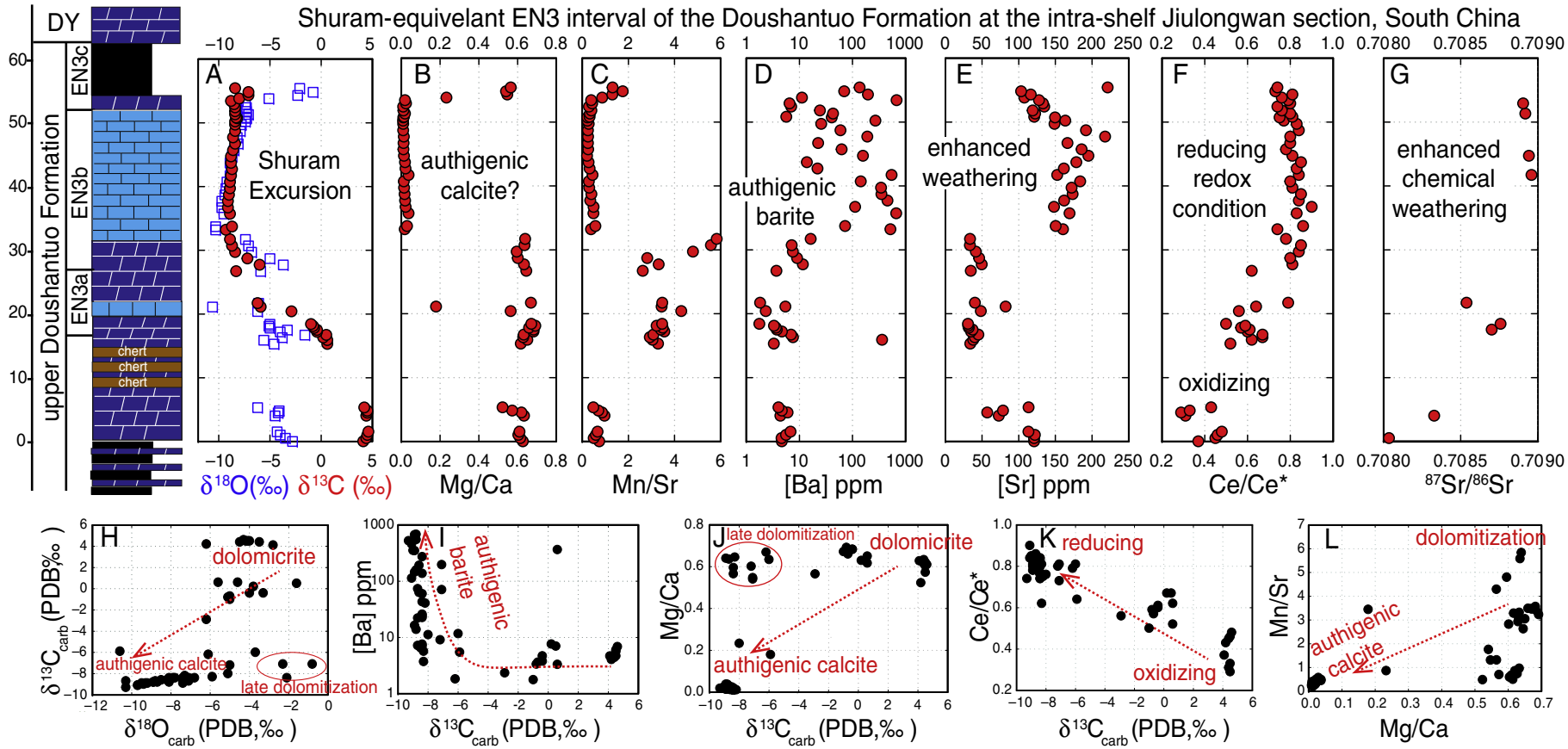

Fig. 14. Geochemical and petrographic data of the upper Doushantuo Formation at the Jiulongwan section. Litho- and chemostratigraphic profiles (A–G) and cross plots (H-L) of the EN3 interval, widely interpreted as equivalent to the Shuram excursion. Barium concentrations [Ba] are new data from this study. Other data are from Zhou et al. (2012). Petrographic studies suggest that samples with high Mg/Ca and Mn/Sr ratios are altered during late dolomitization. In spite of dolomitization of a few samples, the EN3 interval reveals a clear increase in [Sr], [Ba], $^{87}Sr/^{86}Sr$, and Ce/Ce*, suggesting the confluence of enhanced chemical weathering, ocean anoxia, authigenic barite mineralization, and anaerobic oxidation of methane within the SMTZ. All the elemental concentration data plotted in this figure are dissolved with 0.5 N acetic acid. The complete data set can be found in the online supplementary material. Please refer to the supplementary material for detailed field and petrographic observations.

5.5. Shuram Excursion and deep-time carbon cycles

5.5.1. Correlation of the uppermost Doushantuo between Zhongling and Jiulongwan

The variable expression of the $\delta^{13}C$ negative excursion in the uppermost Doushantuo Formation across the basin (Xiao et al., 2012; Lu et al., 2013; Cui et al., 2015; Wang et al., 2016) hampers our interpretation of its origin and global implications (Fig. 8A, J). Construction of composite chemostratigraphic sections should be based on a basin-wide analysis rather than from measurements of any single section. Based on our integrated $\delta^{13}C$–$\delta^{34}S$–$^{87}Sr/^{86}Sr$–Ce/Ce* chemostratigraphy, we noted that EN3 at the Zhongling section and the nearby Yangjiaping section is incompletely preserved, and accordingly we have suggested that the uppermost Doushantuo Formation at Zhongling is likely to be correlated with the EN3a interval at Jiulongwan (Cui et al., 2015, 2016c). Our revised correlation is also consistent with the progressive shallowing in water depth on the basis of independent sedimentological observation in the outer-shelf sections, where an increasing proportion of intraclasts and oolites relative to fine-grained phases are deposited (Jiang et al., 2011; Cui et al., 2015). The missing EN3b and EN3c in the outer-shelf sections may be due to either a basin-wide unconformity (Lu et al., 2013; Zhu et al., 2013; Wang et al., 2016), or the diachronous nature of the lithologic boundary between Doushantuo and Dengying formations (Cui et al., 2015).

If our basin-scale correlation for the Doushantuo Formation is correct, the strongly ^{13}C-depleted authigenic signatures revealed from the uppermost Doushantuo Formation at Zhongling could immediately precedes EN3, or could be time-equivalent to EN3a at the Jiulongwan section, suggesting a potential linkage between methane oxidation, sea level regression, and the onset of the Shuram Excursion (Bjerrum and Canfield, 2011). Indeed, sedimentological observations of the Shuram Excursion from other sections in South China (Lu et al., 2013; Wang et al., 2016), Death Valley (Summa, 1993; Corsetti and Kaufman, 2003; Kaufman et al., 2007; Bergmann et al., 2011), Oman (Fike et al., 2006; Le Guerroué et al., 2006b, 2006c; Lee et al., 2013; Osburn et al., 2014), South Australia (Husson et al., 2012, 2015b), and NW Canada (Macdonald et al., 2013) have also revealed a regression immediately before the onset of the Shuram Excursion, supporting our hypothesis.

5.5.2. Authigenic barite mineralization in SMTZ

Consistent with the interpretation of methane-derived authigenesis at the Zhongling section, the enrichment of barium in the EN3 interval at Jiulongwan further supports an authigenic connection to the Shuram Excursion (Fig. 14). In modern marine sediments, authigenic barite mineralization normally co-occurs with anaerobic oxidation of methane in the SMTZ (Torres et al., 1996; Jørgensen and Kasten, 2006; Riedinger et al., 2006; Feng and Roberts, 2011; Vanneste et al., 2013). When sulfate and organic carbon is available, a barite front forms in the SMTZ where the flux of sulfate diffused from seawater meets with soluble barium diffusing upward from depth. Thus, an enrichment in barium (typically as authigenic barite) has been widely used as an indicator for the reconstruction of paleo SMTZs in deep time records (e.g., Dickens, 2001; Dickens et al., 2003; Lash, 2015; Zhou et al., 2015; Niu et al., 2016). Trace element analyses of the EN3 interval at Jiulongwan reveal a strong enrichment in barium (Fig. 14D). These measurements are consistent with independent sedimentological observations of authigenic barite crystals closely associated with carbonate concretions and black shales (Fig. S3E). The co-occurrence of authigenic calcite and authigenic barite has also been reported in sedimentary rocks deposited during the short-lived Paleocene–Eocene Thermal Maximum (PETM) when gas hydrate dissociation and methane oxidation was believed to have contributed to the negative $\delta^{13}C$ excursion (Dickens, 2001; Dickens et al., 2003).

If the model of a shallow SMTZ is true for the Shuram Excursion, it could explain a variety of sedimentological observations. For example, the Shuram Excursion is globally recorded by bedded micritic limestone (instead of dolomite) independent of sedimentary facies (Melezhik et al., 2009; Grotzinger et al., 2011; Bergmann, 2013; Lu et al., 2013; Husson et al., 2015b). The dominance of limestone in this interval may well reflect an episode of enhanced authigenic mineralization of calcite (or initially aragonite, see Husson et al., 2015a). Abundant seafloor-precipitated aragonite fans (Corsetti and Kaufman, 2003; Pruss et al., 2008; Loyd et al., 2013; see also Greene et al., 2012 for a Phanerozoic analogue), oolite (Corsetti and Kaufman, 2003; Bergmann, 2013), and hummocky cross-stratification (Le Guerroué et al., 2006a, 2006b; Melezhik et al., 2009; Husson et al., 2012) with strong ^{13}C-depletion in the Shuram-equivalent intervals worldwide further support our view of a very shallow (probably near sediment–water interface) SMTZ during the Shuram Excursion.

Heterogeneity in the stratigraphic expression of the Shuram Excursion within individual basins have been reported from the Johnnie Formation in Death Valley (Bergmann et al., 2011), the Gametrail Formation in NW Canada (Macdonald et al., 2013), and the Doushantuo Formation in South China (Jiang et al., 2007, 2008; Lu et al., 2013; Cui et al., 2015; Wang et al., 2016). The development of basin-scale unconformities (Lu et al., 2013; Wang et al., 2016) or mixture of various proportions of authigenic carbonates (Macdonald et al., 2013) have been proposed to explain the intra-basinal heterogeneity in $\delta^{13}C$ expression. Observational evidence for methane-derived authigenesis stratigraphically associated with the Shuram Excursion, however, is currently only limited to the upper Doushantuo Formation at the outer-shelf sections in South China (Ader et al., 2009; Macouin et al., 2012; Cui et al., 2016c; Furuyama et al., 2016 and this study), and perhaps also the Mara Member in the Nama Group of southern Namibia (Kaufman et al., 2015). An active search for these authigenic phases in the fully-expressed Shuram Excursion worldwide may help to further test our hypothesis.

5.5.3. Beyond the Shuram Excursion

Our conceptual model proposed above may shed light on other perturbations of the ancient carbon cycle. These include negative $\delta^{13}C$ fluctuations in the Mesoproterozoic (e.g., Gilleaudeau and Kah, 2013), and early Ediacaran time (e.g., Hoffman et al., 1998; Halverson et al., 2005; Lang et al., 2016), as well as at the Ediacaran–Cambrian boundary (e.g., Maloof et al., 2010a; Maloof et al., 2010b; Jiang et al., 2012), may be explained by the variable admixture of early authigenic carbonates driven by fluctuations of sulfate in the ocean. It is possible that oceanic sulfate concentration was low prior to the Ediacaran Period (Kah et al., 2004; Shen et al., 2006; Kah and Bartley, 2011; Loyd et al., 2012; Crowe et al., 2014) such that methane could have been largely released directly to the ocean and atmosphere rather than being oxidized through microbial metabolism within sediments (e.g., Halverson et al., 2002; Ader et al., 2009; Bristow and Grotzinger, 2013; Li et al., 2015; Shen et al., 2016). As oceanic sulfate level increased in the Ediacaran Period (Fike et al., 2006; Halverson and Hurtgen, 2007; Algeo et al., 2015), however, early authigenic mineralization in shallow marine sediments was enhanced via coupled sulfate reduction and anaerobic oxidation of methane (Jørgensen and Kasten, 2006). Localized, but globally synchronous, production of ^{13}C-depleted authigenic carbonate may have led to the strong negative $\delta^{13}C$ excursions (e.g., Zhou et al., 2016). More detailed studies that combine petrographic, mineralogical, and fabric-specific geochemical investigations (e.g., Talbot and Kelts, 1986; Kozdon et al., 2013; Bojanowski et al., 2015; Lash, 2015; Godet et al., 2016; Śliwiński et al., 2016; Thomazo et al., 2016; Zhao et al., 2016) are needed to test these hypotheses for $\delta^{13}C$ excursions throughout Earth's history.

6. Conclusions

Systematic sedimentological, petrographic, and chemostratigraphic investigations were conducted for the Doushantuo Formation at the outer-shelf Zhongling section in South China. Methane-derived authigenic calcite cement and nodules with extreme ^{13}C-depletion ($\delta^{13}C_{carb}$ down to −37‰) were discovered, and are interpreted as

direct empirical evidence of authigenesis potentially associated with the profound Shuram Excursion. Combined BSE, XRD and isotopic measurements of micro-drilled samples indicate that the cm-scale heterogeneity in $\delta^{13}C_{carb}$ and $\delta^{18}O_{carb}$ reflects the relative abundance of authigenic calcite and depositional dolomite. Based on integrated chemostratigraphic correlation (Cui et al., 2015), these remarkable authigenic signatures at the outer shelf Zhongling section are proposed to be time-equivalent to the EN3a interval of the fully-defined Shuram Excursion at the Jiulongwan section ~90 km to the north, suggesting a potential causal link between methane-derived authigenesis and the globally-expressed Shuram Excursion. In light of these novel observations (Figs. 2–10) and based on our basin-scale chemostratigraphic correlation(Cui et al., 2015), we hypothesize that the Shuram Excursion may be formed by localized, but globally synchronized mineralization of authigenic calcite in a paleo SMTZ located near the sediment–water interface. The onset of this chemocline at the water-sediment interface is believed to be a response to an increase in global seawater sulfate concentrations. Our new conceptual model provides a non-actualistic interpretation for the largest negative $\delta^{13}C$ excursion in Earth history, and suggests a unique geochemical transition in seawater during the Ediacaran Period. Our study highlights the significance of an integrated approach that combines petrography, mineralogy, and texture-specific micro-drilling geochemistry in chemostratigraphic studies. Such approach is suggested to be applied to fully-expressed Shuram-equivalent sections (e.g., the Doushantuo Formation at Jiulongwan) in order to directly test our hypothesis.

Acknowledgements

The authors wish to thank Rebecca Plummer, Yongbo Peng and Mike Evans for their assistance in the UMD Paleoclimate CoLaboratory; Richard Walker, Igor Puchtel and Jingao Liu for the guidance on strontium isotope analysis in the UMD TIMS Laboratory; Peter Zavalij for the assistance on XRD analysis in the UMD X-ray Crystallographic Center; Phil Piccoli, Drew Muscente and Mike Meyer for their assistance on petrographic imaging in the UMD Electron Probe Micro-analyzer (EPMA) Laboratory and the Virginia Tech SEM Laboratory; and Timothy Rose for the guidance on using the Cathodoluminescence Microscope and Spectrometer in the Department of Mineral Sciences, Smithsonian Institution, Washington, DC. We also want to thank Roberta Rudnick, James Farquhar, John Valley, Huifang Xu, Maciej Śliwiński, Kathleen Campbell, Albert Colman, Ganqing Jiang, Chao Li, Genming Luo, Jon Husson, Xianguo Lang, Feifei Zhang, and Yihang Fang for helpful discussion. This manuscript benefited from constructive comments by four anonymous reviewers. Michael Böttcher is also acknowledged for handling this manuscript.

This research is funded by NASA Exobiology (NNX12AR91G to AJK and NNX15AL27G to SX), NSF Sedimentary Geology and Paleontology (EAR0844270 to AJK; EAR1528553 to SX), Chinese Academy of Sciences (KZZD–EW–02 to CZ), and multiple graduate student research grants to HC, including the Mineralogical Society of America (MSA) Grant for Student Research in Mineralogy and Petrology, the Society of Economic Geologists (SEG) Student Research Grant, the Explorers Club Exploration Fund Grant, and the International Association of Sedimentologists (IAS) Graduate Student Research Grant. HC also wants to thank the NASA Astrobiology Institute in UW–Madison for support.

Appendix A. Supplementary data

Supplementary data to this article can be found online at http://dx.doi.org/10.1016/j.chemgeo.2016.12.010.

References

Ader, M., Macouin, M., Trindade, R.I.F., Hadrien, M.-H., Yang, Z., Sun, Z., Besse, J., 2009. A multilayered water column in the Ediacaran Yangtze platform? Insights from carbonate and organic matter paired $\delta^{13}C$. Earth Planet. Sci. Lett. 288, 213–227.

Adkins, J.F., McIntyre, K., Schrag, D.P., 2002. The salinity, temperature, and $\delta^{18}O$ of the glacial deep ocean. Science 298, 1769–1773.

Aharon, P., Schwarcz, H.P., Roberts, H.H., 1997. Radiometric dating of submarine hydrocarbon seeps in the Gulf of Mexico. Geol. Soc. Am. Bull. 109, 568–579.

Ahr, W.M., 2011. Geology of Carbonate Reservoirs: The Identification, Description and Characterization of Hydrocarbon Reservoirs in Carbonate Rocks. John Wiley & Sons.

Algeo, T.J., Luo, G.M., Song, H.Y., Lyons, T.W., Canfield, D.E., 2015. Reconstruction of secular variation in seawater sulfate concentrations. Biogeosciences 12, 2131–2151.

Arthur, M.A., 2009. Carbonate rocks deconstructed. Nature 460, 698–699.

Banner, J.L., Hanson, G.N., 1990. Calculation of simultaneous isotopic and trace element variations during water-rock interaction with applications to carbonate diagenesis. Geochim. Cosmochim. Acta 54, 3123–3137.

Bergmann, K.D., 2013. Constraints on the Carbon Cycle and Climate During the Early Evolution of Animals. California Institute of Technology, Pasadena, California.

Bergmann, K.D., Zentmyer, R.A., Fischer, W.W., 2011. The stratigraphic expression of a large negative carbon isotope excursion from the Ediacaran Johnnie Formation, Death Valley. Precambrian Res. 188, 45–56.

Berner, R.A., 1971. Principles of Chemical Sedimentology. McGraw-Hill, New York.

Berner, R.A., 1981. Authigenic mineral formation resulting from organic matter decomposition in modern sediments. Fortschr. Mineral. 59, 117–135.

Birnbaum, S.J., Wireman, J.W., 1984. Bacterial sulfate reduction and pH: implications for early diagenesis. Chem. Geol. 43, 143–149.

Bishop, J.W., Osleger, D.A., Montañez, I.P., Sumner, D.Y., 2014. Meteoric diagenesis and fluid-rock interaction in the Middle Permian Capitan backreef: Yates Formation, Slaughter Canyon, New Mexico. AAPG Bull. 98, 1495–1519.

Bjerrum, C.J., Canfield, D.E., 2011. Towards a quantitative understanding of the late Neoproterozoic carbon cycle. Proc. Natl. Acad. Sci. 108, 5542–5547.

Bojanowski, M.J., Bagiński, B., Guillermier, C., Franchi, I.A., 2015. Carbon and oxygen isotope analysis of hydrate-associated Oligocene authigenic carbonates using NanoSIMS and IRMS. Chem. Geol. 416, 51–64.

Borowski, W.S., Paull, C.K., Ussler, W., 1996. Marine pore-water sulfate profiles indicate in situ methane flux from underlying gas hydrate. Geology 24, 655–658.

Borowski, W.S., Paull, C.K., Ussler Iii, W., 1999. Global and local variations of interstitial sulfate gradients in deep-water, continental margin sediments: sensitivity to underlying methane and gas hydrates. Mar. Geol. 159, 131–154.

Bottjer, D.J., Hagadorn, J.W., Dornbos, S.Q., 2000. The Cambrian substrate revolution. GSA Today 10, 1–7.

Bristow, T.F., Grotzinger, J.P., 2013. Sulfate availability and the geological record of cold-seep deposits. Geology 41, 811–814.

Bristow, T.F., Bonifacie, M., Derkowski, A., Eiler, J.M., Grotzinger, J.P., 2011. A hydrothermal origin for isotopically anomalous cap dolostone cements from south China. Nature 474, 68–71.

Burns, S.J., Matter, A., 1993. Carbon isotopic record of the latest Proterozoic from Oman. Eclogae Geol. Helv. 86, 595–607.

Burns, S.J., Haudenschild, U., Matter, A., 1994. The strontium isotopic composition of carbonates from the late Precambrian (~560–540 Ma) Huqf Group of Oman. Chem. Geol. 111, 269–282.

Butterfield, N.J., 2009. Oxygen, animals and oceanic ventilation: an alternative view. Geobiology 7, 1–7.

Butterfield, N.J., 2011. Animals and the invention of the Phanerozoic Earth system. Trends Ecol. Evol. 26, 81–87.

Calver, C.R., 2000. Isotope stratigraphy of the Ediacarian (Neoproterozoic III) of the Adelaide Rift Complex, Australia, and the overprint of water column stratification. Precambrian Res. 100, 121–150.

Campbell, K.A., 2006. Hydrocarbon seep and hydrothermal vent paleoenvironments and paleontology: past developments and future research directions. Palaeogeogr. Palaeoclimatol. Palaeoecol. 232, 362–407.

Canfield, D.E., Farquhar, J., 2009. Animal evolution, bioturbation, and the sulfate concentration of the oceans. Proc. Natl. Acad. Sci. 106, 8123–8127.

Canfield, D.E., Poulton, S.W., Knoll, A.H., Narbonne, G.M., Ross, G., Goldberg, T., Strauss, H., 2008. Ferruginous conditions dominated later Neoproterozoic deep-water chemistry. Science 321, 949–952.

Carbone, C., Narbonne, G.M., 2014. When life got smart: the evolution of behavioral complexity through the Ediacaran and early Cambrian of NW Canada. J. Paleontol. 88, 309–330.

Catling, D.C., Claire, M.W., Zahnle, K.J., 2007. Anaerobic methanotrophy and the rise of atmospheric oxygen. Philos. Trans. R. Soc. A Math. Phys. Eng. Sci. 365, 1867–1888.

Chen, Z., Zhou, C., Meyer, M., Xiang, K., Schiffbauer, J.D., Yuan, X., Xiao, S., 2013. Trace fossil evidence for Ediacaran bilaterian animals with complex behaviors. Precambrian Res. 224, 690–701.

Chen, X., Ling, H.-F., Vance, D., Shields-Zhou, G.A., Zhu, M., Poulton, S.W., Och, L.M., Jiang, S.-Y., Li, D., Cremonese, L., Archer, C., 2015. Rise to modern levels of ocean oxygenation coincided with the Cambrian radiation of animals. Nat. Commun. 6, 7142.

Coleman, M.L., Raiswell, R., 1995. Source of carbonate and origin of zonation in pyritiferous carbonate concretions; evaluation of a dynamic model. Am. J. Sci. 295, 282–308.

Condon, D., Zhu, M., Bowring, S., Wang, W., Yang, A., Jin, Y., 2005. U–Pb ages from the Neoproterozoic Doushantuo Formation, China. Science 308, 95–98.

Corsetti, F.A., Kaufman, A.J., 2003. Stratigraphic investigations of carbon isotope anomalies and Neoproterozoic ice ages in Death Valley, California. Geol. Soc. Am. Bull. 115, 916–932.

Crowe, S.A., Paris, G., Katsev, S., Jones, C., Kim, S.-T., Zerkle, A.L., Nomosatryo, S., Fowle, D.A., Adkins, J.F., Sessions, A.L., 2014. Sulfate was a trace constituent of Archean seawater. Science 346, 735–739.

Cui, H., 2015. Authigenesis, Biomineralization, and Carbon–Sulfur Cycling in the Ediacaran Ocean. (Ph.D. dissertation). University of Maryland, College Park.

Cui, H., Kaufman, A.J., Xiao, S., Zhu, M., Zhou, C., Liu, X.-M., 2015. Redox architecture of an Ediacaran ocean margin: Integrated chemostratigraphic ($\delta^{13}C$–$\delta^{34}S$–$^{87}Sr/^{86}Sr$–Ce/Ce*) correlation of the Doushantuo Formation, South China. Chem. Geol. 405, 48–62.

Cui, H., Grazhdankin, D.V., Xiao, S., Peek, S., Rogov, V.I., Bykova, N.V., Sievers, N.E., Liu, X.-M., Kaufman, A.J., 2016a. Redox-dependent distribution of early macro-organisms: evidence from the terminal Ediacaran Khatyspyt Formation in Arctic Siberia. Palaeogeogr. Palaeoclimatol. Palaeoecol. 461, 122–139.

Cui, H., Kaufman, A.J., Xiao, S., Peek, S., Cao, H., Min, X., Cai, Y., Siegel, Z., Liu, X.M., Peng, Y., Schiffbauer, J.D., Martin, A.J., 2016b. Environmental context for the terminal Ediacaran biomineralization of animals. Geobiology 14, 344–363.

Cui, H., Xiao, S., Zhou, C., Peng, Y., Kaufman, A.J., Plummer, R.E., 2016c. Phosphogenesis associated with the Shuram Excursion: petrographic and geochemical observations from the Ediacaran Doushantuo Formation of South China. Sediment. Geol. 341, 134–146.

Davidson, D.W., Leaist, D.G., Hesse, R., 1983. Oxygen-18 enrichment in the water of a clathrate hydrate. Geochim. Cosmochim. Acta 47, 2293–2295.

Degens, E.T., Epstein, S., 1964. Oxygen and carbon isotope ratios in coexisting calcites and dolomites from recent and ancient sediments. Geochim. Cosmochim. Acta 28, 23–44.

Derkowski, A., Bristow, T.F., Wampler, J.M., Środoń, J., Marynowski, L., Elliott, W.C., Chamberlain, C.P., 2013. Hydrothermal alteration of the Ediacaran Doushantuo Formation in the Yangtze Gorges area (South China). Geochim. Cosmochim. Acta 107, 279–298.

Derry, L.A., 2010a. A burial diagenesis origin for the Ediacaran Shuram–Wonoka carbon isotope anomaly. Earth Planet. Sci. Lett. 294, 152–162.

Derry, L.A., 2010b. On the significance of $\delta^{13}C$ correlations in ancient sediments. Earth Planet. Sci. Lett. 296, 497–501.

Dickens, G.R., 2001. Sulfate profiles and barium fronts in sediment on the Blake Ridge: present and past methane fluxes through a large gas hydrate reservoir. Geochim. Cosmochim. Acta 65, 529–543.

Dickens, G.R., Fewless, T., Thomas, E., Bralower, T.J., 2003. Excess barite accumulation during the Paleocene–Eocene Thermal Maximum: massive input of dissolved barium from seafloor gas hydrate reservoirs. Geol. Soc. Am. Spec. Pap. 369, 11–24.

Evans, M., Selmer, K., Breeden, B., Lopatka, A., Plummer, R., 2016. Correction algorithm for on-line continuous flow $\delta^{13}C$ and $\delta^{18}O$ carbonate and cellulose stable isotope analyses. Geochem. Geophys. Geosyst. 17, 3580–3588.

Feng, D., Roberts, H.H., 2011. Geochemical characteristics of the barite deposits at cold seeps from the northern Gulf of Mexico continental slope. Earth Planet. Sci. Lett. 309, 89–99.

Fike, D.A., Grotzinger, J.P., Pratt, L.M., Summons, R.E., 2006. Oxidation of the Ediacaran ocean. Nature 444, 744–747.

Furuyama, S., Kano, A., Kunimitsu, Y., Ishikawa, T., Wei, W., 2016. Diagenetic overprint to a negative carbon isotope anomaly associated with the Gaskiers glaciation of the Ediacaran Doushantuo Formation in South China. Precambrian Res. 110–122.

Gilleaudeau, G.J., Kah, L.C., 2013. Carbon isotope records in a Mesoproterozoic epicratonic sea: carbon cycling in a low-oxygen world. Precambrian Res. 228, 85–101.

Glenn, C.R., Föllmi, K.B., Riggs, S.R., Baturin, G.N., Grimm, K.A., Trappe, J., Abed, A.M., Galli-Oliver, C., Garrison, R.E., Ilyan, A., Jehl, C., Rohrlich, V., Sadaqah, R.M., Schidlowski, M., Sheldon, R.E., Siegmund, H., 1994. Phosphorus and phosphorites: sedimentology and environments of formation. Eclogae Geol. Helv. 87, 747–788.

Glenn, C.R., Prévôt-Lucas, L., Lucas, J., 2000. Marine authigenesis: from global to microbial. SEPM Special Publication No. 66. SEPM (Society for Sedimentary Geology), Tullsa, Oklahoma, USA.

Godet, A., Durlet, C., Spangenberg, J.E., Föllmi, K.B., 2016. Estimating the impact of early diagenesis on isotope records in shallow-marine carbonates: a case study from the Urgonian Platform in western Swiss Jura. Palaeogeogr. Palaeoclimatol. Palaeoecol. 454, 125–138.

Gomez, F.J., Kah, L.C., Bartley, J.K., Astini, R.A., 2014. Microbialites in a high-altitude Andean lake: multiple controls in carbonate precipitation and lamina accretion. PALAIOS 29, 233–249.

Greene, S.E., Bottjer, D.J., Corsetti, F.A., Berelson, W.M., Zonneveld, J.-P., 2012. A subseafloor carbonate factory across the Triassic–Jurassic transition. Geology 40, 1043–1046.

Greinert, J., Bohrmann, G., Suess, E., 2001. Gas hydrate-associated carbonates and methane-venting at Hydrate Ridge: classification, distribution, and origin of authigenic lithologies. In: Paull, C.K., Dillon, W.P. (Eds.), Natural Gas Hydrates: Occurrence, Distribution, and Detection. American Geophysical Union, Washington, D. C., pp. 99–113.

Gross, M.G., Tracey, J.I., 1966. Oxygen and carbon isotopic composition of limestones and dolomites, bikini and eniwetok atolls. Science 151, 1082–1084.

Grotzinger, J.P., Fike, D.A., Fischer, W.W., 2011. Enigmatic origin of the largest-known carbon isotope excursion in Earth's history. Nat. Geosci. 4, 285–292.

Habicht, K.S., Gade, M., Thamdrup, B., Berg, P., Canfield, D.E., 2002. Calibration of sulfate levels in the Archean ocean. Science 298, 2372–2374.

Haeckel, M., Suess, E., Wallmann, K., Rickert, D., 2004. Rising methane gas bubbles form massive hydrate layers at the seafloor. Geochim. Cosmochim. Acta 68, 4335–4345.

Hall, M., Kaufman, A.J., Vickers-Rich, P., Ivantsov, A., Trusler, P., Linnemann, U., Hofmann, M., Elliott, D., Cui, H., Fedonkin, M., Hoffmann, K.-H., Wilson, S.A., Schneider, G., Smith, J., 2013. Stratigraphy, palaeontology and geochemistry of the late Neoproterozoic Aar Member, southwest Namibia: reflecting environmental controls on Ediacara fossil preservation during the terminal Proterozoic in African Gondwana. Precambrian Res. 238, 214–232.

Halverson, G.P., Hurtgen, M.T., 2007. Ediacaran growth of the marine sulfate reservoir. Earth Planet. Sci. Lett. 263, 32–44.

Halverson, G.P., Hoffman, P.F., Schrag, D.P., Kaufman, A.J., 2002. A major perturbation of the carbon cycle before the Ghaub glaciation (Neoproterozoic) in Namibia: prelude to snowball Earth? Geochem. Geophys. Geosyst. 3, 1–24.

Halverson, G.P., Hoffman, P.F., Schrag, D.P., Maloof, A.C., Rice, A.H.N., 2005. Toward a Neoproterozoic composite carbon-isotope record. Geol. Soc. Am. Bull. 117, 1181–1207.

Hayes, J.M., 1994. Global methanotrophy at the Archean-Proterozoic transition. In: Bengtson, S. (Ed.), Early Life on Earth. Nobel Symposium No. 84. Columbia University Press, New York, pp. 220–236.

Hayes, J.M., Waldbauer, J.R., 2006. The carbon cycle and associated redox processes through time. Philos. Trans. R. Soc. B Biol. Sci. 361, 931–950.

Higgins, J., Fischer, W., Schrag, D., 2009. Oxygenation of the ocean and sediments: consequences for the seafloor carbonate factory. Earth Planet. Sci. Lett. 284, 25–33.

Hoffman, P.F., Kaufman, A.J., Halverson, G.P., Schrag, D.P., 1998. A Neoproterozoic snowball earth. Science 281, 1342–1346.

Hohl, S., Becker, H., Herzlieb, S., Guo, Q., 2015. Multiproxy constraints on alteration and primary compositions of Ediacaran deep-water carbonate rocks, Yangtze Platform, South China. Geochim. Cosmochim. Acta 163, 262–278.

Horita, J., 2014. Oxygen and carbon isotope fractionation in the system dolomite-water-CO_2 to elevated temperatures. Geochim. Cosmochim. Acta 129, 111–124.

Horton, T.W., Defliese, W.F., Tripati, A.K., Oze, C., 2015. Evaporation induced ^{18}O and ^{13}C enrichment in lake systems: a global perspective on hydrologic balance effects. Quat. Sci. Rev. 365–379.

Hovland, M., Talbot, M.R., Qvale, H., Olaussen, S., Aasberg, L., 1987. Methane-related carbonate cements in pockmarks of the North Sea. J. Sediment. Res. 57, 881–892.

Huang, J., Chu, X., Jiang, G., Feng, L., Chang, H., 2011. Hydrothermal origin of elevated iron, manganese and redox-sensitive trace elements in the *c.* 635 Ma Doushantuo cap carbonate. J. Geol. Soc. 168, 805–816.

Husson, J.M., Maloof, A.C., Schoene, B., 2012. A syn-depositional age for Earth's deepest $\delta^{13}C$ excursion required by isotope conglomerate tests. Terra Nova 24, 318–325.

Husson, J.M., Higgins, J.A., Maloof, A.C., Schoene, B., 2015a. Ca and Mg isotope constraints on the origin of Earth's deepest C excursion. Geochim. Cosmochim. Acta 160, 243–266.

Husson, J.M., Maloof, A.C., Schoene, B., Chen, C.Y., Higgins, J.A., 2015b. Stratigraphic expression of Earth's deepest $\delta^{13}C$ excursion in the Wonoka Formation of South Australia. Am. J. Sci. 315, 1–45.

Jacobsen, S.B., Kaufman, A.J., 1999. The Sr, C and O isotopic evolution of Neoproterozoic seawater. Chem. Geol. 161, 37–57.

Jaffrés, J.B., Shields, G.A., Wallmann, K., 2007. The oxygen isotope evolution of seawater: a critical review of a long-standing controversy and an improved geological water cycle model for the past 3.4 billion years. Earth Sci. Rev. 83, 83–122.

Jiang, G., Kennedy, M.J., Christie-Blick, N., 2003. Stable isotopic evidence for methane seeps in Neoproterozoic postglacial cap carbonates. Nature 426, 822–826.

Jiang, G., Kennedy, M.J., Christie-Blick, N., Wu, H., Zhang, S., 2006a. Stratigraphy, sedimentary structures, and textures of the late Neoproterozoic Doushantuo cap carbonate in South China. J. Sediment. Res. 76, 978–995.

Jiang, G., Shi, X., Zhang, S., 2006b. Methane seeps, methane hydrate destabilization, and the late Neoproterozoic postglacial cap carbonates. Chin. Sci. Bull. 51, 1152–1173.

Jiang, G., Kaufman, A.J., Christie-Blick, N., Zhang, S., Wu, H., 2007. Carbon isotope variability across the Ediacaran Yangtze platform in South China: implications for a large surface-to-deep ocean $\delta^{13}C$ gradient. Earth Planet. Sci. Lett. 261, 303–320.

Jiang, G., Zhang, S., Shi, X., Wang, X., 2008. Chemocline instability and isotope variations of the Ediacaran Doushantuo basin in South China. Sci. China Ser. D Earth Sci. 51, 1560–1569.

Jiang, G., Shi, X., Zhang, S., Wang, Y., Xiao, S., 2011. Stratigraphy and paleogeography of the Ediacaran Doushantuo Formation (ca. 635–551 Ma) in South China. Gondwana Res. 19, 831–849.

Jiang, G., Wang, X., Shi, X., Xiao, S., Zhang, S., Dong, J., 2012. The origin of decoupled carbonate and organic carbon isotope signatures in the early Cambrian (ca. 542–520 Ma) Yangtze platform. Earth Planet. Sci. Lett. 317–318, 96–110.

Jørgensen, B.B., 1982. Mineralization of organic matter in the sea bed—the role of sulphate reduction. Nature 296, 643–645.

Jørgensen, B.B., Kasten, S., 2006. Sulfur cycling and methane oxidation. In: Schulz, H.D., Zabel, M. (Eds.), Marine Geochemistry. Springer-Verlag, Heidelberg, Berlin, pp. 271–309.

Joseph, C., Torres, M., Martin, R., Haley, B., Pohlman, J., Riedel, M., Rose, K., 2012. Using the $^{87}Sr/^{86}Sr$ of modern and paleoseep carbonates from northern Cascadia to link modern fluid flow to the past. Chem. Geol. 334, 122–130.

Kah, L.C., 2000. Depositional $\delta^{18}O$ signatures in Proterozoic dolostones: constraints on seawater chemistry and early diagenesis. In: Grotzinger, J.P., James, N.P. (Eds.), Carbonate Sedimentation and Diagenesis in the Evolving Precambrian World. SEPM Society for Sedimentary Geology, Tulsa, Oklahoma, USA, pp. 245–260.

Kah, L.C., Bartley, J.K., 2011. Protracted oxygenation of the Proterozoic biosphere. Int. Geol. Rev. 53, 1424–1442.

Kah, L.C., Lyons, T.W., Frank, T.D., 2004. Low marine sulphate and protracted oxygenation of the Proterozoic biosphere. Nature 431, 834–838.

Kasting, J.F., Howard, M.T., Wallmann, K., Veizer, J., Shields, G., Jaffrés, J., 2006. Paleoclimates, ocean depth, and the oxygen isotopic composition of seawater. Earth Planet. Sci. Lett. 252, 82–93.

Kastner, M., 1999. Oceanic minerals: their origin, nature of their environment, and significance. Proc. Natl. Acad. Sci. 96, 3380–3387.

Kaufman, A.J., Corsetti, F.A., Varni, M.A., 2007. The effect of rising atmospheric oxygen on carbon and sulfur isotope anomalies in the Neoproterozoic Johnnie Formation, Death Valley, USA. Chem. Geol. 237, 47–63.

Kaufman, A.J., Kriesfeld, L., Cui, H., Narbonne, G.M., Vickers-Rich, P., Zhou, C., Xiao, S., 2015. An authigenic origin for the middle Ediacaran Shuram excursion: The view from Namibia and South China. 2015 GSA Annual Meeting. The Geological Society of America, Baltimore, Maryland, USA, p. 451.

Kennedy, M., Mrofka, D., von der Borch, C., 2008. Snowball Earth termination by destabilization of equatorial permafrost methane clathrate. Nature 453, 642–645.
Knauth, L.P., 2005. Temperature and salinity history of the Precambrian ocean: implications for the course of microbial evolution. Palaeogeogr. Palaeoclimatol. Palaeoecol. 219, 53–69.
Knauth, L.P., Kennedy, M.J., 2009. The late Precambrian greening of the Earth. Nature 460, 728–732.
Kozdon, R., Kelly, D., Kitajima, K., Strickland, A., Fournelle, J., Valley, J., 2013. In situ $\delta^{18}O$ and Mg/Ca analyses of diagenetic and planktic foraminiferal calcite preserved in a deep-sea record of the Paleocene–Eocene thermal maximum. Paleoceanography 28, 517–528.
Kump, L.R., Arthur, M.A., 1999. Interpreting carbon-isotope excursions: carbonates and organic matter. Chem. Geol. 161, 181–198.
Lang, X., Shen, B., Peng, Y., Huang, K., Lv, J., Ma, H., 2016. Ocean oxidation during the deposition of basal Ediacaran Doushantuo cap carbonates in the Yangtze Platform, South China. Precambrian Res. 281, 253–268.
Langmuir, D., Hall, P., Drever, J., 1997. Environmental Geochemistry. Prentice Hall, New Jersey.
Lash, G.G., 2015. Authigenic barite nodules and carbonate concretions in the Upper Devonian shale succession of western New York – a record of variable methane flux during burial. Mar. Pet. Geol. 59, 305–319.
Le Guerroué, E., 2006. Sedimentology and Chemostratigraphy of the Ediacaran Shuram Formation, Nafun Group, Oman. Eidgenössische Technische Hochschule Zürich (ETHZ), Zürich, Switzerland.
Le Guerroué, E., Allen, P.A., Cozzi, A., 2006a. Parasequence development in the Ediacaran Shuram Formation (Nafun Group, Oman): high-resolution stratigraphic test for primary origin of negative carbon isotopic ratios. Basin Res. 18, 205–219.
Le Guerroué, E., Allen, P.A., Cozzi, A., 2006b. Chemostratigraphic and sedimentological framework of the largest negative carbon isotopic excursion in Earth history: The Neoproterozoic Shuram Formation (Nafun Group, Oman). Precambrian Res. 146, 68–92.
Le Guerroué, E., Allen, P.A., Cozzi, A., Etienne, J.L., Fanning, M., 2006c. 50 Myr recovery from the largest negative $\delta^{13}C$ excursion in the Ediacaran ocean. Terra Nova 18, 147–153.
Lee, C., Fike, D.A., Love, G.D., Sessions, A.L., Grotzinger, J.P., Summons, R.E., Fischer, W.W., 2013. Carbon isotopes and lipid biomarkers from organic-rich facies of the Shuram Formation, Sultanate of Oman. Geobiology 11, 406–419.
Lee, C., Love, G.D., Fischer, W.W., Grotzinger, J.P., Halverson, G.P., 2015. Marine organic matter cycling during the Ediacaran Shuram excursion. Geology 43, 1103–1106.
Lein, A.Y., 2004. Authigenic carbonate formation in the ocean. Lithol. Miner. Resour. 39, 1–30.
Lenton, T.M., Boyle, R.A., Poulton, S.W., Shields-Zhou, G.A., Butterfield, N.J., 2014. Co-evolution of eukaryotes and ocean oxygenation in the Neoproterozoic era. Nat. Geosci. 7, 257–265.
Li, H.C., Ku, T.L., 1997. $\delta^{13}C$–$\delta^{18}C$ covariance as a paleohydrological indicator for closed-basin lakes. Palaeogeogr. Palaeoclimatol. Palaeoecol. 133, 69–80.
Li, C., Love, G.D., Lyons, T.W., Fike, D.A., Sessions, A.L., Chu, X., 2010. A stratified redox model for the Ediacaran ocean. Science 328, 80–83.
Li, C., Planavsky, N.J., Love, G.D., Reinhard, C.T., Hardisty, D., Feng, L., Bates, S.M., Huang, J., Zhang, Q., Chu, X., Lyons, T.W., 2015. Marine redox conditions in the middle Proterozoic ocean and isotopic constraints on authigenic carbonate formation: Insights from the Chuanlinggou Formation, Yanshan Basin, North China. Geochim. Cosmochim. Acta 150, 90–105.
Li, F.-B., Teng, F.-Z., Chen, J.-T., Huang, K.-J., Wang, S.-J., Lang, X.-G., Ma, H.-R., Peng, Y.-B., Shen, B., 2016. Constraining ribbon rock dolomitization by Mg isotopes: implications for the 'dolomite problem'. Chem. Geol. 445, 208–220.
Lin, Z., Wang, Q., Feng, D., Liu, Q., Chen, D., 2011. Post-depositional origin of highly ^{13}C-depleted carbonate in the Doushantuo cap dolostone in South China: insights from petrography and stable carbon isotopes. Sediment. Geol. 242, 71–79.
Liu, X.-M., Kah, L.C., Knoll, A.H., Cui, H., Kaufman, A.J., Shahar, A., Hazen, R.M., 2016. Tracing Earth's O_2 evolution using Zn/Fe ratios in marine carbonates. Geochem. Perspect. Lett. 2, 24–34.
Logan, G.A., Hayes, J., Hieshima, G.B., Summons, R.E., 1995. Terminal Proterozoic reorganization of biogeochemical cycles. Nature 376, 53–56.
Lohmann, K.C., 1988. Geochemical patterns of meteoric diagenetic systems and their application to studies of paleokarst. In: James, N.P., Choquette, P.W. (Eds.), Paleokarst. Springer-Verlag, New York City, pp. 58–80.
Loyd, S.J., Marenco, P.J., Hagadorn, J.W., Lyons, T.W., Kaufman, A.J., Sour-Tovar, F., Corsetti, F.A., 2012. Sustained low marine sulfate concentrations from the Neoproterozoic to the Cambrian: insights from carbonates of northwestern Mexico and eastern California. Earth Planet. Sci. Lett. 339–340, 79–94.
Loyd, S.J., Marenco, P.J., Hagadorn, J.W., Lyons, T.W., Kaufman, A.J., Sour-Tovar, F., Corsetti, F.A., 2013. Local $\delta^{34}S$ variability in ~580 Ma carbonates of northwestern Mexico and the Neoproterozoic marine sulfate reservoir. Precambrian Res. 224, 551–569.
Loyd, S.J., Corsetti, F.A., Eagle, R.A., Hagadorn, J.W., Shen, Y., Zhang, X., Bonifacie, M., Tripati, A.K., 2015. Evolution of Neoproterozoic Wonoka–Shuram Anomaly-aged carbonates: evidence from clumped isotope paleothermometry. Precambrian Res. 264, 179–191.
Lu, M., Zhu, M., Zhang, J., Shields-Zhou, G., Li, G., Zhao, F., Zhao, X., Zhao, M., 2013. The DOUNCE event at the top of the Ediacaran Doushantuo Formation, South China: Broad stratigraphic occurrence and non-diagenetic origin. Precambrian Res. 225, 86–109.
Lyons, T.W., Reinhard, C.T., Planavsky, N.J., 2014. The rise of oxygen in Earth's early ocean and atmosphere. Nature 506, 307–315.
Macdonald, F.A., Strauss, J.V., Sperling, E.A., Halverson, G.P., Narbonne, G.M., Johnston, D.T., Kunzmann, M., Schrag, D.P., Higgins, J.A., 2013. The stratigraphic relationship between the Shuram carbon isotope excursion, the oxygenation of Neoproterozoic oceans, and the first appearance of the Ediacara biota and bilaterian trace fossils in northwestern Canada. Chem. Geol. 362, 250–272.
Macouin, M., Ader, M., Moreau, M.-G., Poitou, C., Yang, Z., Sun, Z., 2012. Deciphering the impact of diagenesis overprint on negative $\delta^{13}C$ excursions using rock magnetism: case study of Ediacaran carbonates, Yangjiaping section, South China. Earth Planet. Sci. Lett. 351–352, 281–294.
Maloof, A.C., Porter, S.M., Moore, J.L., Dudás, F.Ö., Bowring, S.A., Higgins, J.A., Fike, D.A., Eddy, M.P., 2010a. The earliest Cambrian record of animals and ocean geochemical change. Geol. Soc. Am. Bull. 122, 1731–1774.
Maloof, A.C., Ramezani, J., Bowring, S.A., Fike, D.A., Porter, S.M., Mazouad, M., 2010b. Constraints on early Cambrian carbon cycling from the duration of the Nemakit-Daldynian–Tommotian boundary $\delta^{13}C$ shift, Morocco. Geology 38, 623–626.
Marshall, J.D., 1992. Climatic and oceanographic isotopic signals from the carbonate rock record and their preservation. Geol. Mag. 129, 143–160.
McFadden, K.A., Huang, J., Chu, X., Jiang, G., Kaufman, A.J., Zhou, C., Yuan, X., Xiao, S., 2008. Pulsed oxidation and biological evolution in the Ediacaran Doushantuo Formation. Proc. Natl. Acad. Sci. 105, 3197–3202.
McMurtry, G.M., 2009. Authigenic deposits. In: Steele, J.H., Thorpe, S.A., Turekian, K.K. (Eds.), Marine Chemistry & Geochemistry: A Derivative of the Encyclopedia of Ocean Sciences, second ed. Elsevier, Oxford, pp. 325–335.
Meister, P., 2013. Two opposing effects of sulfate reduction on carbonate precipitation in normal marine, hypersaline, and alkaline environments. Geology 41, 499–502.
Meister, P., 2015. For the deep biosphere, the present is not always the key to the past: what we can learn from the geological record. Terra Nova 27, 400–408.
Melezhik, V.A., Fallick, A.E., Smith, R.A., Rosse, D.M., 2007. Spherical and columnar, septarian, ^{18}O-depleted, calcite concretions from Middle–Upper Permian lacustrine siltstones in northern Mozambique: evidence for very early diagenesis and multiple fluids. Sedimentology 54, 1389–1416.
Melezhik, V.A., Pokrovsky, B.G., Fallick, A.E., Kuznetsov, A.B., Bujakaite, M.I., 2009. Constraints on $^{87}Sr/^{86}Sr$ of Late Ediacaran seawater: insight from Siberian high-Sr limestones. J. Geol. Soc. 166, 183–191.
Metzger, J.G., Fike, D.A., 2013. Techniques for assessing spatial heterogeneity of carbonate $\delta^{13}C$ values: Implications for craton-wide isotope gradients. Sedimentology 60, 1405–1431.
Mishra, P.K., Prasad, S., Anoop, A., Plessen, B., Jehangir, A., Gaye, B., Menzel, P., Weise, S.M., Yousuf, A.R., 2015. Carbonate isotopes from high altitude Tso Moriri Lake (NW Himalayas) provide clues to late glacial and Holocene moisture source and atmospheric circulation changes. Palaeogeogr. Palaeoclimatol. Palaeoecol. 425, 76–83.
Moore, C.H., 1989. Carbonate Diagenesis and Porosity, 46. Elsevier.
Moore, C.H., 2004. Carbonate Reservoirs: Porosity Evolution and Diagenesis in a Sequence Stratigraphic Framework.
Moore, T.S., Murray, R., Kurtz, A., Schrag, D., 2004. Anaerobic methane oxidation and the formation of dolomite. Earth Planet. Sci. Lett. 229, 141–154.
Morad, S., Ketzer, J.M., De Ros, L.F., 2013. Linking Diagenesis to Sequence Stratigraphy: An Integrated Tool for Understanding and Predicting Reservoir Quality Distribution. John Wiley & Sons, Inc. (1-36 pp.).
Morse, J., 2003. Formation and diagenesis of carbonate sediments. In: Holland, H.D., Turekian, K.K. (Eds.), Treatise on Geochemistry, Volume 7: Sediments, Diagenesis, and Sedimentary Rocks. Elsevier, Oxford, pp. 67–85.
Morse, J.W., Mackenzie, F.T., 1990. Geochemistry of Sedimentary Carbonates. Elsevier, Amsterdam.
Mozley, P.S., Burns, S.J., 1993. Oxygen and carbon isotopic composition of marine carbonate concretions: an overview. J. Sediment. Res. 63, 73–83.
Muehlenbachs, K., 1998. The oxygen isotopic composition of the oceans, sediments and the seafloor. Chem. Geol. 145, 263–273.
Muehlenbachs, K., Clayton, R.N., 1976. Oxygen isotope composition of the oceanic crust and its bearing on seawater. J. Geophys. Res. 81, 4365–4369.
Muscente, A.D., Hawkins, A.D., Xiao, S., 2015. Fossil preservation through phosphatization and silicification in the Ediacaran Doushantuo Formation (South China): a comparative synthesis. Palaeogeogr. Palaeoclimatol. Palaeoecol. 434, 46–62.
Naehr, T.H., Rodriguez, N.M., Bohrmann, G., Paull, C.K., Botz, R., 2000. Methane-derived authigenic carbonates associated with gas hydrate decomposition and fluid venting above the Blake Ridge Diapir. In: Paull, C.K., Matsumoto, R., Wallace, P.J., Dillon, W.P. (Eds.), Proceedings of the Ocean Drilling Program. Scientific Results. Ocean Drilling Program, pp. 285–300.
Narbonne, G.M., Xiao, S., Shields, G.A., Gehling, J.G., 2012. The Ediacaran Period. In: Gradstein, F.M., Ogg, J.G., Schmitz, M.D., Ogg, G.M. (Eds.), The Geologic Time Scale. Elsevier, Boston, pp. 413–435.
Niu, D., Renock, D., Whitehouse, M., Leone, J., Rowe, H., Landis, J., Hamren, K., Symcox, C.W., Sharma, M., 2016. A relict sulfate–methane transition zone in the mid-Devonian Marcellus Shale. Geochim. Cosmochim. Acta 182, 73–87.
Northrop, D.A., Clayton, R.N., 1966. Oxygen-isotope fractionations in systems containing dolomite. J. Geol. 174–196.
Nyman, S.L., Nelson, C.S., 2011. The place of tubular concretions in hydrocarbon cold seep systems: Late Miocene Urenui Formation, Taranaki Basin, New Zealand. AAPG Bull. 95, 1495–1524.
Oehlert, A.M., Swart, P.K., 2014. Interpreting carbonate and organic carbon isotope covariance in the sedimentary record. Nat. Commun. 5, 4672.
O'Neil, J.R., Epstein, S., 1966. Oxygen isotope fractionation in the system dolomite-calcite-carbon dioxide. Science 152, 198–201.
Osburn, M., Grotzinger, J., Bergmann, K., 2014. Facies, stratigraphy, and evolution of a middle Ediacaran carbonate ramp: Khufai Formation, Sultanate of Oman. AAPG Bull. 98, 1631–1667.
Osburn, M.R., Owens, J., Bergmann, K.D., Lyons, T.W., Grotzinger, J.P., 2015. Dynamic changes in sulfate sulfur isotopes preceding the Ediacaran Shuram Excursion. Geochim. Cosmochim. Acta 170, 204–224.
Pavlov, A.A., Hurtgen, M.T., Kasting, J.F., Arthur, M.A., 2003. Methane-rich Proterozoic atmosphere? Geology 31, 87–90.

Peckmann, J., Reimer, A., Luth, U., Luth, C., Hansen, B.T., Heinicke, C., Hoefs, J., Reitner, J., 2001. Methane-derived carbonates and authigenic pyrite from the northwestern Black Sea. Mar. Geol. 177, 129–150.

Peng, Y., Bao, H., Zhou, C., Yuan, X., Luo, T., 2013. Oxygen isotope composition of meltwater from a Neoproterozoic glaciation in South China. Geology 41, 367–370.

Planavsky, N.J., Reinhard, C.T., Wang, X., Thomson, D., McGoldrick, P., Rainbird, R.H., Johnson, T., Fischer, W.W., Lyons, T.W., 2014. Low Mid-Proterozoic atmospheric oxygen levels and the delayed rise of animals. Science 346, 635–638.

Pruss, S.B., Corsetti, F.A., Fischer, W.W., 2008. Seafloor-precipitated carbonate fans in the Neoproterozoic Rainstorm Member, Johnnie Formation, Death Valley Region, USA. Sediment. Geol. 207, 34–40.

Quinn, T.M., 1991. Meteoric diagenesis of Plio-Pleistocene limestones at Enewetak atoll. J. Sediment. Res. 61, 681–703.

Riedinger, N., Kasten, S., Gröger, J., Franke, C., Pfeifer, K., 2006. Active and buried authigenic barite fronts in sediments from the Eastern Cape Basin. Earth Planet. Sci. Lett. 241, 876–887.

Riedinger, N., Formolo, M.J., Lyons, T.W., Henkel, S., Beck, A., Kasten, S., 2014. An inorganic geochemical argument for coupled anaerobic oxidation of methane and iron reduction in marine sediments. Geobiology 12, 172–181.

Ritger, S., Carson, B., Suess, E., 1987. Methane-derived authigenic carbonates formed by subduction-induced pore-water expulsion along the Oregon/Washington margin. Geol. Soc. Am. Bull. 98, 147–156.

Rohling, E.J., 2007. Oxygen isotope composition of seawater. In: A. E.S . (Ed.), Encyclopedia of Quaternary Science. Elsevier, Amsterdam, pp. 915–922.

Saitoh, M., Ueno, Y., Isozaki, Y., Shibuya, T., Yao, J., Ji, Z., Shozugawa, K., Matsuo, M., Yoshida, N., 2015. Authigenic carbonate precipitation at the end-Guadalupian (Middle Permian) in China: implications for the carbon cycle in ancient anoxic oceans. Prog. Earth Planet. Sci. 2, 41.

Sass, E., Bein, A., Almogi-Labin, A., 1991. Oxygen-isotope composition of diagenetic calcite in organic-rich rocks: evidence for ^{18}O depletion in marine anaerobic pore water. Geology 19, 839–842.

Sawaki, Y., Ohno, T., Tahata, M., Komiya, T., Hirata, T., Maruyama, S., Windley, B.F., Han, J., Shu, D., Li, Y., 2010. The Ediacaran radiogenic Sr isotope excursion in the Doushantuo Formation in the Three Gorges area, South China. Precambrian Res. 176, 46–64.

Schidlowski, M., 1987. Application of stable carbon isotopes to early biochemical evolution on Earth. Annu. Rev. Earth Planet. Sci. 15, 47–72.

Schmitz, M.D., 2012. Radiometric ages used in GTS2012. In: Gradstein, F.M., Ogg, J.G., Schmitz, M.D., Ogg, G.M. (Eds.), The Geologic Time Scale. Elsevier, Boston, pp. 1045–1082.

Schobben, M., Ullmann, C.V., Leda, L., Korn, D., Struck, U., Reimold, W.U., Ghaderi, A., Algeo, T.J., Korte, C., 2016. Discerning primary versus diagenetic signals in carbonate carbon and oxygen isotope records: an example from the Permian–Triassic boundary of Iran. Chem. Geol. 422, 94–107.

Schrag, D.P., Higgins, J.A., Macdonald, F.A., Johnston, D.T., 2013. Authigenic carbonate and the history of the global carbon cycle. Science 339, 540–543.

Shaffer, G., 1986. Phosphate pumps and shuttles in the Black Sea. Nature 321, 515–517.

Shen, Y., Pinti, D.L., Hashizume, K., 2006. Biogeochemical cycles of sulfur and nitrogen in the Archean ocean and atmosphere. Archean Geodyn. Environ. 305–320.

Shen, B., Dong, L., Xiao, S., Lang, X., Huang, K., Peng, Y., Zhou, C., Ke, S., Liu, P., 2016. Molar tooth carbonates and benthic methane fluxes in Proterozoic oceans. Nat. Commun. 7, 10317.

Sheppard, S.M.F., Schwarcz, H.P., 1970. Fractionation of carbon and oxygen isotopes and magnesium between coexisting metamorphic calcite and dolomite. Contrib. Mineral. Petrol. 26, 161–198.

Śliwiński, M.G., Kozdon, R., Kitajima, K., Valley, J.W., Denny, A., 2016. Microanalysis of carbonate cement $\delta^{18}O$ in a CO_2-storage system seal: insights into the diagenetic history of the Eau Claire Formation (Upper Cambrian), Illinois Basin. AAPG Bull. 1003–1031.

Sperling, E.A., Wolock, C.J., Morgan, A.S., Gill, B.C., Kunzmann, M., Halverson, G.P., Macdonald, F.A., Knoll, A.H., Johnston, D.T., 2015. Statistical analysis of iron geochemical data suggests limited late Proterozoic oxygenation. Nature 523, 451–454.

Spero, H.J., Bijma, J., Lea, D.W., Bemis, B.E., 1997. Effect of seawater carbonate concentration on foraminiferal carbon and oxygen isotopes. Nature 390, 497–500.

Suess, E., 2014. Marine cold seeps and their manifestations: geological control, biogeochemical criteria and environmental conditions. Int. J. Earth Sci. 103, 1889–1916.

Summa, C.L., 1993. Sedimentologic, Stratigraphic, and Tectonic Controls of a Mixed Carbonate-Siliciclastic Succession: Neoproterozoic Johnnie Formation, Southeast California. Massachusetts Institute of Technology.

Sun, X., Turchyn, A.V., 2014. Significant contribution of authigenic carbonate to marine carbon burial. Nat. Geosci. 7, 201–204.

Swart, P.K., Kennedy, M.J., 2012. Does the global stratigraphic reproducibility of $\delta^{13}C$ in Neoproterozoic carbonates require a marine origin? A Pliocene–Pleistocene comparison. Geology 40, 87–90.

Tahata, M., Ueno, Y., Ishikawa, T., Sawaki, Y., Murakami, K., Han, J., Shu, D., Li, Y., Guo, J., Yoshida, N., Komiya, T., 2013. Carbon and oxygen isotope chemostratigraphies of the Yangtze platform, South China: decoding temperature and environmental changes through the Ediacaran. Gondwana Res. 23, 333–353.

Talbot, M., Kelts, K., 1986. Primary and diagenetic carbonates in the anoxic sediments of Lake Bosumtwi, Ghana. Geology 14, 912–916.

Teichert, B.M., Gussone, N., Eisenhauer, A., Bohrmann, G., 2005. Clathrites: archives of near-seafloor pore-fluid evolution ($\delta^{44/40}Ca$, $\delta^{13}C$, $\delta^{18}O$) in gas hydrate environments. Geology 33, 213–216.

Thomazo, C., Vennin, E., Brayard, A., Bour, I., Mathieu, O., Elmeknassi, S., Olivier, N., Escarguel, G., Bylund, K.G., Jenks, J., Stephen, D.A., Fara, E., 2016. A diagenetic control on the Early Triassic Smithian–Spathian carbon isotopic excursions recorded in the marine settings of the Thaynes Group (Utah, USA). Geobiology 14, 220–236.

Torres, M.E., Brumsack, H., Bohrmann, G., Emeis, K., 1996. Barite fronts in continental margin sediments: a new look at barium remobilization in the zone of sulfate reduction and formation of heavy barites in diagenetic fronts. Chem. Geol. 127, 125–139.

Tucker, M.E., 1982. Precambrian dolomites: petrographic and isotopic evidence that they differ from Phanerozoic dolomites. Geology 10, 7–12.

Tucker, M.E., 1983. Diagenesis, geochemistry, and origin of a Precambrian dolomite: the Beck Spring Dolomite of eastern California. J. Sediment. Res. 53, 1097–1119.

Tucker, M.E., Wright, V.P., 1990. Carbonate Sedimentology. Blackwell Scientific Publications, Oxford.

Vanneste, H., James, R.H., Kelly-Gerreyn, B.A., Mills, R.A., 2013. Authigenic barite records of methane seepage at the Carlos Ribeiro mud volcano (Gulf of Cadiz). Chem. Geol. 354, 42–54.

Veizer, J., Bruckschen, P., Pawellek, F., Diener, A., Podlaha, O.G., Carden, G.A., Jasper, T., Korte, C., Strauss, H., Azmy, K., 1997. Oxygen isotope evolution of Phanerozoic seawater. Palaeogeogr. Palaeoclimatol. Palaeoecol. 132, 159–172.

Veizer, J., Ala, D., Azmy, K., Bruckschen, P., Buhl, D., Bruhn, F., Carden, G.A., Diener, A., Ebneth, S., Godderis, Y., 1999. $^{87}Sr/^{86}Sr$, $\delta^{13}C$ and $\delta^{18}O$ evolution of Phanerozoic seawater. Chem. Geol. 161, 59–88.

Walter, L.M., Burton, E.A., 1990. Dissolution of recent platform carbonate sediments in marine pore fluids. Am. J. Sci. 290, 601–643.

Walter, L.M., Bischof, S.A., Patterson, W.P., Lyons, T.W., O'Nions, R., Gruszczynski, M., Sellwood, B., Coleman, M., 1993. Dissolution and recrystallization in modern shelf carbonates: evidence from pore water and solid phase chemistry [and discussion]. Philos. Trans. R. Soc. Lond. A Math. Phys. Eng. Sci. 344, 27–36.

Wang, J., Jiang, G., Xiao, S., Li, Q., Wei, Q., 2008. Carbon isotope evidence for widespread methane seeps in the ca. 635 Ma Doushantuo cap carbonate in south China. Geology 36, 347–350.

Wang, W., Zhou, C., Guan, C., Yuan, X., Chen, Z., Wan, B., 2014. An integrated carbon, oxygen, and strontium isotopic studies of the Lantian Formation in South China with implications for the Shuram anomaly. Chem. Geol. 373, 10–26.

Wang, X., Jiang, G., Shi, X., Xiao, S., 2016. Paired carbonate and organic carbon isotope variations of the Ediacaran Doushantuo Formation from an upper slope section at Siduping, South China. Precambrian Res. 273, 53–66.

Watkins, J.M., Hunt, J.D., Ryerson, F.J., DePaolo, D.J., 2014. The influence of temperature, pH, and growth rate on the $\delta^{18}O$ composition of inorganically precipitated calcite. Earth Planet. Sci. Lett. 404, 332–343.

Wright, V.P., Cherns, L., 2016. Leaving no stone unturned: the feedback between increased biotic diversity and early diagenesis during the Ordovician. J. Geol. Soc. 173, 241–244.

Xiao, S., Schiffbauer, J.D., McFadden, K.A., Hunter, J., 2010. Petrographic and SIMS pyrite sulfur isotope analyses of Ediacaran chert nodules: Implications for microbial processes in pyrite rim formation, silicification, and exceptional fossil preservation. Earth Planet. Sci. Lett. 297, 481–495.

Xiao, S., McFadden, K.A., Peek, S., Kaufman, A.J., Zhou, C., Jiang, G., Hu, J., 2012. Integrated chemostratigraphy of the Doushantuo Formation at the northern Xiaofenghe section (Yangtze Gorges, South China) and its implication for Ediacaran stratigraphic correlation and ocean redox models. Precambrian Res. 192–195, 125–141.

Xiao, S., Narbonne, G.M., Zhou, C., Laflamme, M., Grazhdankin, D.V., Moczydłowska-Vidal, M., Cui, H., 2016. Toward an Ediacaran time scale: problems, protocols, and prospects. Episodes 39, 540–555.

Xu, H., 2010. Synergistic roles of microorganisms in mineral precipitates associated with deep sea methane seeps. In: Barton, L.L., Mandl, M., Loy, A. (Eds.), Geomicrobiology: Molecular and Environmental Perspective. Springer, Berlin, Germany, pp. 325–346.

Zhao, Y.-Y., Zheng, Y.-F., 2010. Stable isotope evidence for involvement of deglacial meltwater in Ediacaran carbonates in South China. Chem. Geol. 271, 86–100.

Zhao, Y.-Y., Zheng, Y.-F., 2015. Geochemistry of vein and wallrock carbonates from the Ediacaran system in South China: insights into the origins of depositional and post-depositional fluids. Chem. Geol. 404, 71–87.

Zhao, M.-Y., Zheng, Y.-F., Zhao, Y.-Y., 2016. Seeking a geochemical identifier for authigenic carbonate. Nat. Commun. 7, 10885.

Zhelezinskaia, I., Kaufman, A.J., Farquhar, J., Cliff, J., 2014. Large sulfur isotope fractionations associated with Neoarchean microbial sulfate reduction. Science 346, 742–744.

Zhou, C., Xiao, S., 2007. Ediacaran $\delta^{13}C$ chemostratigraphy of South China. Chem. Geol. 237, 89–108.

Zhou, C., Bao, H., Peng, Y., Yuan, X., 2010. Timing the deposition of ^{17}O-depleted barite at the aftermath of Nantuo glacial meltdown in South China. Geology 38, 903–906.

Zhou, C., Jiang, S., Xiao, S., Chen, Z., Yuan, X., 2012. Rare earth elements and carbon isotope geochemistry of the Doushantuo Formation in South China: implication for middle Ediacaran shallow marine redox conditions. Chin. Sci. Bull. 57, 1998–2006.

Zhou, X., Chen, D., Dong, S., Zhang, Y., Guo, Z., Wei, H., Yu, H., 2015. Diagenetic barite deposits in the Yurtus Formation in Tarim Basin, NW China: implications for barium and sulfur cycling in the earliest Cambrian. Precambrian Res. 263, 79–87.

Zhou, C., Guan, C., Cui, H., Ouyang, Q., Wang, W., 2016. Methane-derived authigenic carbonate from the lower Doushantuo Formation of South China: implications for seawater sulfate concentration and global carbon cycle in the early Ediacaran ocean. Palaeogeogr. Palaeoclimatol. Palaeoecol. 461, 145–155.

Zhu, M., Zhang, J., Yang, A., 2007. Integrated Ediacaran (Sinian) chronostratigraphy of South China. Palaeogeogr. Palaeoclimatol. Palaeoecol. 254, 7–61.

Zhu, M., Lu, M., Zhang, J., Zhao, F., Li, G., Yang, A., Zhao, X., Zhao, M., 2013. Carbon isotope chemostratigraphy and sedimentary facies evolution of the Ediacaran Doushantuo Formation in western Hubei, South China. Precambrian Res. 225, 7–28.